https://doi.org/10.5194/egusphere-2024-3491
Preprint. Discussion started: 15 November 2024

Evaluating the Feasibility of Scaling the FIER Framework for Large-Scale Flood Inundation Prediction

Kel N. Markert[1,2], Hyongki Lee[3], Gustavious P. Williams[2], E. James Nelson[2], Daniel P. Ames[2], Robert E. Griffin[4], Franz J. Meyer[5]

[1]Google LLC, Mountain View, CA 94043, USA
[2]Department of Civil and Construction Engineering, Brigham Young University, Provo, UT 84602, USA
[3]Department of Civil and Environmental Engineering, University of Houston, Houston, TX 77204, USA
[4]Department of Atmospheric and Earth Science, University of Alabama in Huntsville, Huntsville, AL 35899, USA
[5]Geophysical Institute, University of Alaska Fairbanks, Fairbanks, AK, USA

Correspondence to: Kel N. Markert (kmarkert@google.com)

Abstract. Floods are a recurring global threat, causing lives lost, property damage, and agricultural impacts. Accurate and timely flood inundation forecasts are crucial for effective disaster preparedness and mitigation. However, traditional flood forecasting methods often face challenges in terms of computational demands and data requirements, particularly when applied to large geographic areas. This study presents a novel approach to scaling a data-driven flood forecasting framework, Forecasting Inundation Extents using REOF (Rotated Empirical Orthogonal Function) (FIER), to large geographic regions. FIER leverages historical satellite imagery and streamflow data to predict flood inundation extents without relying on complex hydrodynamic models. We demonstrate the effectiveness of applying FIER over a large geographic extent using watershed boundaries to create individual FIER models and then mosaicking the results geographically to provide large flood inundation predictions. The Upper Mississippi Alluvial Plain in the United States was used as a test region. We evaluated multiple buffer sizes for watersheds for generating the data-driven FIER models to reduce edge effects along watershed boundaries when mosaicking the individual FIER implementations. The FIER method using watersheds, coupled with different forecast lead times from the National Water Model operational streamflow forecasts, was used to accurately predict the extent of surface water for select flood and low flow use cases. Our results show that the scaled FIER approach using watersheds yields higher accuracies for different error metrics, including the Structural Similarity Index Measure (SSIM), RMSE, and MAE. The metrics for the watershed-scaling approach resulted in SSIM ranging from 0.699-0.804, RMSE range of 7.15- 8.60, and an MAE range of 1.09-1.88 compared to a baseline area with SSIM ranging from 0.643-0.693, RMSE range of 8.112- 11.681, and an MAE range of 1.969-1.989. We found that scaling FIER using a watershed approach yielded statistically significant better performance compared to the baseline area: this is particularly true when using buffer sizes for the watersheds of 0-10km and when applying a post-processing correction to the FIER outputs. This approach offers a promising solution for large-scale flood forecasting, particularly in data-scarce regions or ungauged basins. Future research will focus on refining the framework to incorporate additional hydrological variables and improve the accuracy of long-range flood inundation predictions.

https://doi.org/10.5194/egusphere-2024-3491
Preprint. Discussion started: 15 November 2024

1 Introduction

Natural disasters, with flooding the most prevalent, are estimated to cause over $300 billion in annual direct asset losses globally (Hallegatte et al. 2017). A recent study by the World Bank suggests that 1.47 billion people, or 19 percent of the world population, are directly exposed to substantial risks during 1-in-100-year flood events. Of these 1.47 billion people exposed to flood risk, 89 percent live in low- and middle-income countries (Rentschler and Salhab, 2020). Climate change projections for 2030 indicate that the proportion of the population exposed to floods will increase (Tellman et al., 2021). Since 1980, 42 riverine and urban flooding events in the United States have cost a total of $197.2B (on average $4.4B per year) (Smith, 2020). Research has found that flood exposure and damages in the U.S. could also be exacerbated in the future due to anthropogenic climate change, population growth, and urban development (Tate et al., 2021; Wing et al., 2022). Accurate and timely forecasts that capture the spatiotemporal evolution of flood inundations with sufficient lead time for actions are crucial for mitigating the devastating impacts of floods on communities and infrastructure.

Hydrodynamic modeling is a widely used method for simulating the spatiotemporal behavior of flood inundation by creating inundation maps computed from modeled streamflow (Teng et al., 2017). These hydrodynamic models are highly sensitive to inputs, including the streamflow, the boundary and initial conditions, the digital elevation model (DEM) used, and friction coefficients, all of which are difficult to obtain and have associated variation and uncertainty. These uncertainties in hydrodynamic model calibration and data inputs significantly influence the uncertainty of flood inundation predictions (Bates et al., 2014; Teng et al., 2017) with the inundation extent estimates most sensitive to topography and friction coefficients (Yalcin, 2020). Hydrodynamic models carry a heavy computational burden, especially for a more accurate high-resolution large-scale forecasting framework, that could affect forecast lead-time and accuracy (Ben-Haim et al., 2019). While continental-scale hydrodynamic models such as LISFLOOD-FP (Sampson et al., 2012), CaMa-Flood (Yamazaki et al., 2011), or HyMAP (Getirana et al., 2012) are more computationally efficient and have been successfully implemented at large scale, they are typically run as “offline” models or are set up to run at a coarse resolution (1 - 25 km resolution) which limits the use for operational flood inundation purposes at the local level. Even these more efficient models still require detailed parameterization, which can introduce errors, making them impractical in some cases due to data requirements, uncertainty, and complexity.

An area of active research in flood forecasting leverages advancements in Earth observations and machine learning to enhance prediction accuracy and provide spatially explicit inundation information. Data-driven approaches are being explored to establish relationships between rainfall forecasts, satellite-observed inundation patterns, and other hydrometeorological variables, enabling more efficient and potentially accurate flood extent predictions. For example, a recent study published methods for forecasting inundation extent using Earth observation data, such as rainfall forecasts with machine learning approaches to estimate water fraction (Du et al., 2021). Another example that uses machine learning to estimate flood inundation extent is the Google Flood Forecasting system (Nevo et al., 2022), which trains a per-pixel thresholding algorithm on historical satellite observations of flooding. Indeed, integrating historical satellite data, machine

https://doi.org/10.5194/egusphere-2024-3491
Preprint. Discussion started: 15 November 2024

learning algorithms, and hydrologic model outputs offers a promising avenue for developing robust flood forecasting systems.

A promising data-driven framework for predicting surface water extents using satellite and hydrologic data is the Forecasting Inundation Extents using Rotated Empirical Orthogonal Function (FIER) framework (Chang et al., 2020). This framework operates by extracting historical patterns to identify recurring spatial and temporal patterns of flooding using a statistical technique called Rotated Empirical Orthogonal Function (REOF) analysis (Kaiser, 1958). Then these flood patterns are then correlated with historical hydrological data (e.g., streamflow, water levels) to build regression models. Using simulated (retrospective or forecast) hydrological data as input, FIER synthesizes corresponding flood maps. The main advantages of this framework are its computational efficiency, scalability, and ability to operate in data-scarce regions. FIER implementations are typically trained on and applied to specific regions, limiting their applicability to broader areas. Hydrological regimes, topography, and flood characteristics vary significantly across different geographical locations, requiring regionally tailored implementations for accurate predictions. This is due to FIER being a data driven method meaning that the method is dependent on the data inputs and the patterns it can extract from the data. FIER has been applied to the Mekong Delta (Chang et al., 2023) and small regions in the US (Rostami, et al. in review) but it is unknown how the method will perform when attempting to develop the model for very large areas (e.g.,all of the Mississippi basin) when there may be varying patterns of floods. Moreover, there is a computational challenge as the nature of developing the flood patterns requires loading data in memory for processing so applying FIER over large areas can be a challenge. Expanding the spatial coverage of FIER is crucial for the applicability of the method for an operational product over large areas.

This paper explores the feasibility of applying FIER in a manner that creates a consistent flood forecast for large areas making the methods applicable for operational use. We apply FIER for multiple watersheds across a large area and test combining them to create a seamless surface water predictions. The results of the method are compared against a baseline implementation of FIER for a single area to compare how the combination for large area simulation compares to the traditional methods. The technical implementation and statistical validation are described. Furthermore, we provided additional analysis to highlight the method's capability to provide accurate flood forecasts. This approach has the potential to be highly beneficial for operational flood forecasting and can contribute to more effective decision-making in the events of floods. By enabling the application of FIER to large river basins with diverse flood characteristics, this research paves the way for developing robust, computationally efficient flood inundation forecasting systems worldwide, particularly in data-scarce regions where traditional hydrodynamic models are often infeasible.

2 Details on the FIER framework

The FIER framework offers a novel approach to flood inundation forecasting, leveraging a data-driven method to produce spatial flood inundation estimates without the complexities and computational needs of traditional hydrodynamic models. At its core, FIER establishes a statistical relationship between historical flood patterns, derived from satellite imagery, and

https://doi.org/10.5194/egusphere-2024-3491
Preprint. Discussion started: 15 November 2024

corresponding hydrological data, typically streamflow or water levels. This relationship is then used to predict historical and future flood extents based on modeled hydrological conditions.

The FIER process begins by applying Empirical Orthogonal Functions (EOF) (Lorenz, 1956) to a multi-temporal stack of satellite images that capture historical flood events. EOF, a variant of Principal Component Analysis (PCA), decomposes the spatiotemporal variability of the images into a set of orthogonal spatial patterns, and their corresponding temporal variations. The original images can be reconstructed by weighted combinations of these components. In many cases the signal from any individual component may not be significantly different from random noise, therefore a Monte Carlo significance test (Hannachi, 2004) is performed to identify the significant components. The extracted significant components that are retained represent truncated information. In some fields physical meaning can be assigned to components, but the extracted significant components may not contain isolated signals, meaning individual components are hard to interpret as physical processes (Dommenget and Latif, 2002), therefore a rotation is applied, in this case the varimax rotation, which changes the orientation of the factors without altering their fit to the data to obtain simple structures. This makes it easier to physically interpret the inundation patterns in the components. The process of rotating the EOF is known as Rotated Empirical Orthogonal Function (REOF) analysis. The resulting spatial patterns are termed Rotated Spatial Modes (RSMs) whereas their corresponding temporal variations are called Rotated Temporal Principal Components (RTPCs). Each RSM represents a distinct spatial pattern, while its associated RTPC describes how that pattern evolves over time. Next, a correlation analysis is performed that identifies the RTPCs that are significantly correlated with the hydrological data, representing flood-relevant modes. Regression models are then built to link these flood-relevant RTPCs to the corresponding hydrological variable. These regression models can consist of using generalized linear models (Chang et al., 2020) or more sophisticated machine learning/deep learning approaches (Chang et al., 2023). To forecast flood inundation, forecasted hydrological data are used as the input into the trained regression models to predict future RTPCs. These predicted RTPCs are then multiplied by their corresponding RSMs and summed to synthesize a forecasted flood signal (essentially a reverse PCA), which can be further processed to generate a map of predicted flood extent. Figure 1 displays a flowchart schematic which summarizes the FIER process, readers are directed to (Chang et al., 2020, 2023) for additional details on the FIER process.

https://doi.org/10.5194/egusphere-2024-3491
Preprint. Discussion started: 15 November 2024

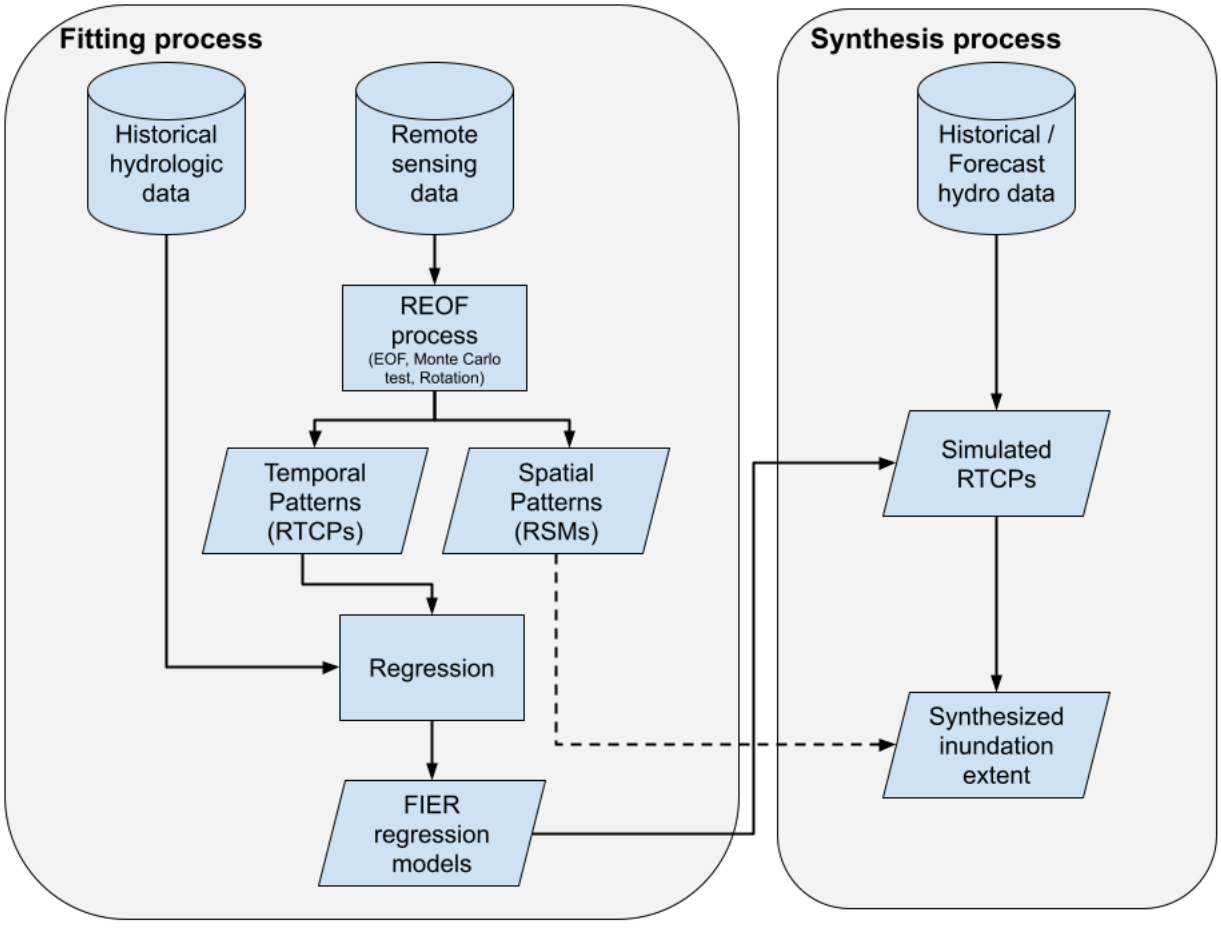

Figure 1: Schematic of the FIER workflow. Adapted from (Rostami, et al. in review).

Scaling the FIER approach to larger geographic extents presents several challenges. One key limitation is the diminishing signal of floods as the area of analysis increases. FIER relies on identifying recurring spatial patterns of flooding from satellite imagery. As the area expands, these patterns become less distinct and more challenging to extract, particularly in regions with diverse hydrological regimes or where flooding is not widespread. This can lead to reduced accuracy and difficulty in establishing robust relationships between flood patterns and hydrological variables because the REOF process may extract other signals occurring on the land surface.

Additionally, computational challenges arise when processing large volumes of satellite data and performing REOF analysis over extensive areas. The FIER implementation requires significant computational resources and processing time when applied to large areas at regional to continental scales. For example, applying the REOF process over large areas requires

https://doi.org/10.5194/egusphere-2024-3491
Preprint. Discussion started: 15 November 2024

reading in an entire time series of satellite imagery into memory and applying the PCA and REOF process over massive arrays. This challenge limits its applicability to select organizations with such computational resources and hinders its operational feasibility due to computational needs and runtime. These limitations necessitate exploring alternative approaches, such as the proposed watershed-based scaling method, to overcome the diminishing flood signal and computational bottlenecks associated with scaling FIER to larger geographic extents.

3 Materials & Methods

3.1 Study Area

This study focuses on a flood plain as part of the lower Mississippi basin, more specifically the region extending from approximately St. Louis, Missouri past Memphis, Tennessee. This region was selected because it is characterized by extensive floodplains along the Mississippi River and complex network of tributaries which also experience flooding. The confluence of multiple major rivers occurs in the region including the Mississippi, Ohio, Tennessee, and Cumberland Rivers. Furthermore, there are reservoirs within the region which are used for hydropower generation and to regulate flow into the Mississippi River to reduce flooding. Flood events in the lower Mississippi area are primarily triggered by rainfall and snowmelt. More recently, the region is experiencing a shift in climate leading to increases in streamflow (Yin et al., 2023). In 2011 and 2019 there were flooding events related to heavy precipitation and late spring snowmelt (Gledhill et al., 2020) where the recent flood event in 2019 was regarded as one of the longest lasting events in the past century (Pal et al., 2020). All these factors lead to a complex hydrology for the region making it an ideal candidate for testing the scalability of the FIER method.

Figure 2 shows the study area along with historical average (2012-2020) surface water fraction derived from the Visible Infrared Imaging Radiometer Suite (VIIRS) sensors. The study uses two subsets of the broader region for testing the methods: 1) a baseline region and 2) the watersheds surrounding the baseline region (see details in section 2.3 Experimental Design for further explanation on the two subregions). The baseline region is marked in red whereas the watersheds are shown with the black outlines.

https://doi.org/10.5194/egusphere-2024-3491
Preprint. Discussion started: 15 November 2024

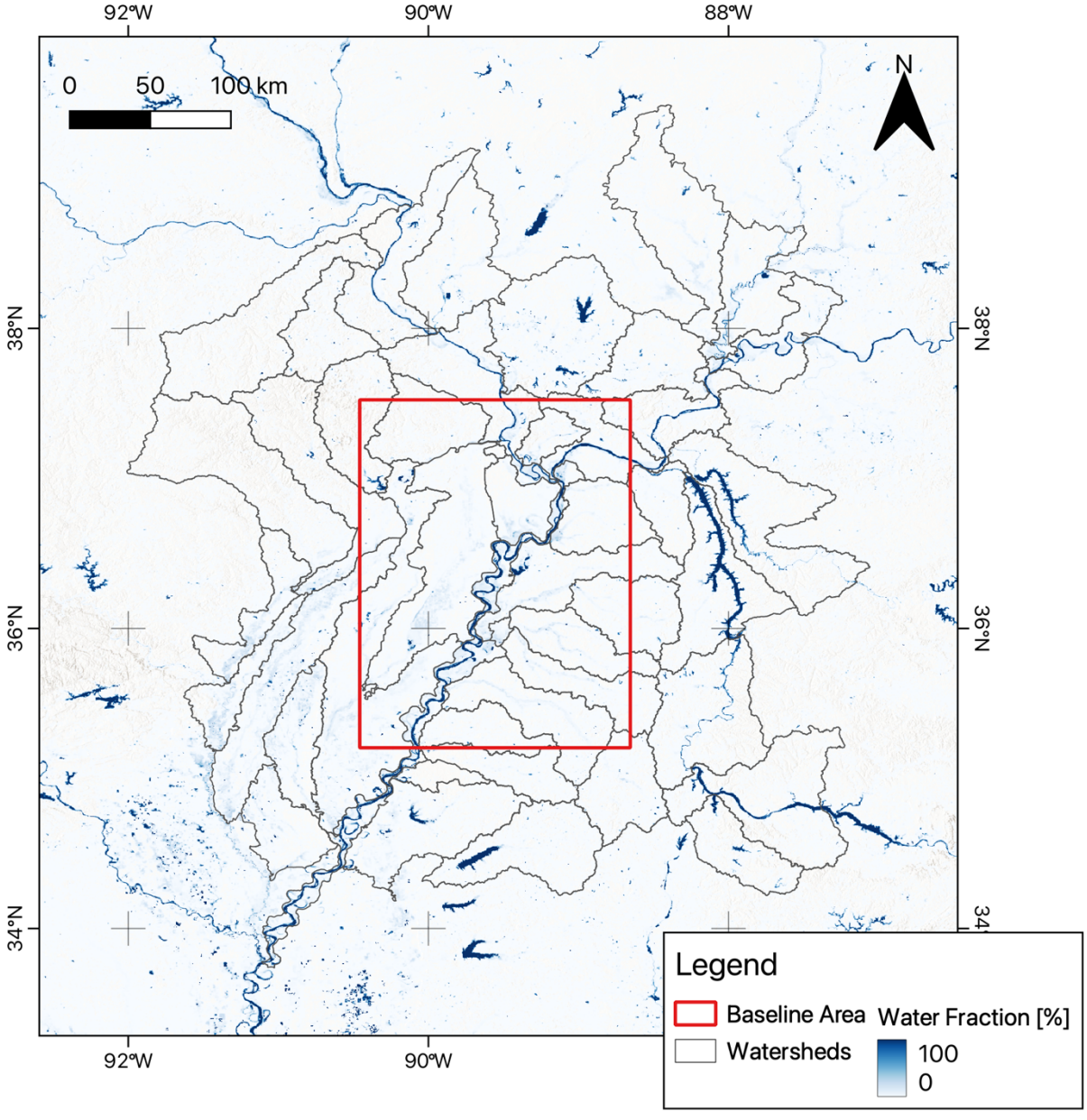

Figure 2: Study area map showing the average surface water fraction derived from the VIIRS sensor from 2012-2020 along with two subregions, the baseline region for FIER in red and the surrounding watersheds in black.

https://doi.org/10.5194/egusphere-2024-3491
Preprint. Discussion started: 15 November 2024

3.2 Data

The Visible Infrared Imaging Radiometer Suite (VIIRS) is an optical sensor onboard the Suomi-NPP, NOAA-20, and NOAA-21 satellites. The VIIRS sensors provide images with a spatial resolution of 375 meters across five spectral bands ranging from visible to thermal infrared channels and has a swath width of 3000 km with a consistent across-scan spatial resolution. These sensor characteristics ensure more comprehensive global daily coverage and make it more favorable than the MODIS data for flood mapping (Li et al., 2020, 2022). The National Oceanic and Atmospheric Administration (NOAA) uses the VIIRS imagery from the three satellites to produce an operational daily surface water fraction estimate for the entire globe (Li et al., 2018). The VIIRS water fraction product produced by NOAA was used to extract the spatiotemporal patterns of surface water and flood changes using the FIER framework. These data were accessed from the AWS Registry of Open Data, specifically the NOAA Joint Polar Satellite System (JPSS) cloud storage bucket (https://registry.opendata.aws/noaa-jpss/). The data were ingested into Google Earth Engine (Gorelick et al., 2017) as an ImageCollection. Earth Engine was used to preprocess the VIIRS data and extract data cubes in the format required for processing with FIER. We used the full record of VIIRS water fraction maps for the study, 2012-01-20 to, however the VIIRS water fraction data has a missing period from 2021-01-01 to 2023-08-10 that was excluded from the study.

We used the National Water Model (NWM) streamflow data as the hydrologic variable to predict the flood-relevant temporal patterns with FIER. The NWM (Cosgrove et al., 2024) is a hydrologic modeling framework developed by NOAA at the National Water Center in Tuscaloosa, Alabama that simulates streamflow data for over 2.7 million river reaches across the United States along with other hydrologic information such as snow water equivalent and soil moisture. The NWM forecasts include two datasets, the retrospective dataset which is a historical simulation from 1979 to 2023 and the operational dataset which is run every day to produce operational forecasts since late 2018. The operational dataset includes a short-range 18-h deterministic forecast that provides flow estimates on an hourly time step, a medium-range forecast with 10 days (member 1) and 8.5 days (members 2–6) with a 3-h time step and a long-range 30-day four-member ensemble forecast on a 6-h time step. The short-range forecast is initialized every hour and the medium- and long-range forecasts are initialized every 6 h. In addition to the forecast runs there is also an analysis and assimilation run which is a nowcast of current streamflow conditions that includes data assimilation from streamflow gauges and a run with no data assimilation. We used both NWM datasets in this study; the retrospective data version 3.0 were used to fit the FIER temporal components to the historical simulated streamflow whereas the operational products were used to predict flood extent for select cases. The retrospective data was accessed through the AWS Registry of Open Data from the NOAA National Water Model CONUS Retrospective Dataset (https://registry.opendata.aws/nwm-archive/). The operational data was accessed via the Google Cloud Public Dataset on BigQuery (Markert et al., 2024b).

https://doi.org/10.5194/egusphere-2024-3491
Preprint. Discussion started: 15 November 2024

3.3 Experimental Design

The experimental design for this study aims to evaluate the effectiveness and accuracy of scaling the FIER method across larger spatial extents. We tested two approaches: applying FIER to a singular baseline area encompassing a portion of the study area, which is used as the control, and applying FIER multiple watersheds individually before mosaicking the results together. The study area was subdivided into 46 smaller watersheds using HUC8 watershed boundaries (see Fig. 4.2 for geographical representation of the watersheds). This comparison is meant to assess whether dividing the region to run FIER individually and then mosaicking together impacts the accuracy of the flood predictions. Given that the FIER method is data-driven where the patterns it can extract, and the results of flood inundation are based on the data inputs. This can cause edge effects along watershed boundaries when mosaicking the individual FIER implementations. To mitigate potential edge effects and ensure smooth transitions between mosaicked watershed predictions, varying buffer sizes (0, 1, 2, 5, 10, 20, and 50 km) were tested when processing individual watersheds. Multiple buffer sizes were tested to determine the optimal buffer size for minimizing discrepancies at watershed boundaries.

The FIER framework requires that all pixels in a time-series be present to use to extract patterns, therefore only imagery with 99.9% clear sky conditions were used to limit the gaps in space for the extracted spatial patterns. Water fractions were predicted and evaluated using dates where the observed imagery had a greater than 90% clear sky conditions. The dates used for training were not evaluated for performance and used only to fit the FIER framework.

FIER predictions use truncated information from the modes that are correlated with hydrologic variables, meaning mathematically the predicted water fraction cannot maintain its original scale of 0 to 100%. Other research (Rostami et al, in review) have applied a quantile mapping method to the FIER predictions which restore the complete signal range as much as possible. Quantile mapping is widely used in climate and hydrology studies to correct the biases in model-estimated values (Enayati et al., 2020; Farmer et al., 2018). The method matches the quantiles of Cumulative Distribution Functions (CDFs) from the predicted to the observed. The CDFs were calculated for all FIER trials (baseline and different buffers) using only the dates that were used for training on a per-pixel basis. The quantile mapping post-processing was applied for the prediction dates for all FIER trials. The two versions of FIER outputs, the original FIER predictions and post-processed predictions utilizing quantile mapping, were evaluated. This allows for evaluating the impact of post-processing on the accuracy of the mosaicked results compared to the baseline.

3.4 Statistical Analysis

To effectively compare the different experiments with the baseline, a statistical analysis was performed to understand and compare the accuracies as well as test if there are statistical differences between the experiments and baseline. The accuracy assessment employs multiple metrics: Structural Similarity Index Measure (SSIM) (Wang et al., 2004) to assess the spatial accuracy of flood extents, Root Mean Square Error (RMSE) to quantify the accuracy of intensity of flood predictions,

https://doi.org/10.5194/egusphere-2024-3491
Preprint. Discussion started: 15 November 2024

Relative RMSE to assess the errors relative to the observed value, and lastly Mean Absolute Error (MAE) as another statistical measure to quantify the accuracy of intensity of flood predictions (Jackson et al., 2019).

The SSIM metric is defined by equation 1:

$$SSIM(x,y) = \frac{(2\mu_x\mu_x+C_1)(2\sigma_{xy}+c_2)}{(\mu_x^2+\mu_y^2+C_1)(\sigma_x^2+\sigma_y^2+C_2)}, \quad (1)$$

Where μ_x is the pixel sample mean of x, μ_y is the pixel sample mean of y, σ_x^2 is the variance of x, σ_y^2 the variance of y, σ_{xy} is the covariance of x and y, x is the test image, y is the reference image, $c_1=(k_1L)^2$, $c_2=(k_2L)^2$ two variables to stabilize the division with weak denominator, L is the dynamic range of the pixel-values (in this case 100 to represent the range of water fraction), $k1=0.01$ and $k2=0.03$ by default. The SSIM index is calculated on various windows of an image, in this case we used an 11x11 gaussian kernel for the calculation, and then averaged across the image to get the final SSIM metric. The SSIM has a range of -1 to 1 where 1 indicates perfect similarity, 0 indicates no similarity, and -1 indicates perfect anti-correlation.

The RMSE metric is calculated using equation 2:

$$RMSE = \sqrt{\frac{1}{n}\sum_i^n (x_i - y_i)^2}, \quad (2)$$

Where x_i are the observations, y_i are the observed values, and n is the number of observations.

The RRMSE metric is calculated using equation 3:

$$RRMSE = \sqrt{\frac{\frac{1}{n}\sum_i^n (x_i-y_i)^2}{\frac{1}{n}\sum_i^n (y_i{}^2)}}, \quad (3)$$

Lastly, the MAE is defined as equation 4:

$$MAE = \frac{1}{n}\sum_i^n |x_i - y_i|, \quad (4)$$

These error metrics were calculated for each pixel comparing the predictions to the observed and then averaged across the baseline area for each date of prediction. The baseline area was used to calculate the metric averages to keep the area consistent between the baseline and mosaicked results so that the results can be compared without influence of different areas.

The last statistical test used was the Kolmogorov-Smirnov test (Massey, 1951) to statistically compare the distributions of the evaluation metrics between the baseline and mosaicked results for both original and post-processed FIER outputs. This test compares whether two samples came from the same distribution. The test was performed for each metric and for every buffer size but keeping the baseline consistent. Lastly, the one-sided test was used to identify whether a given error metric was statistically greater than or less than the baseline. For the SSIM metric we tested if the mosaicked predictions are

https://doi.org/10.5194/egusphere-2024-3491
Preprint. Discussion started: 15 November 2024

significantly greater than the baseline. For the other error metrics (RSME, RRMSE, MAE) we tested if the mosaicked predictions are significantly lower than the baseline.

3.5 Case Studies

The statistical analysis described in the previous section was done using retrospective NWM streamflow as inputs into FIER, however, running FIER for actual flood extents will involve using the operational NWM streamflow predictions. Using case studies serves to provide an evaluation of using the operational NWM for specific flood and low flow cases. We selected the statistically best FIER experiment for running the use cases.

To identify dates to use as cases for the low flow example, we selected a representative reach within the region close to the center of the baseline region along the Mississippi River. The streamflow data for the representative reach was averaged by month. The months with the lowest streamflow for 2019 and 2020 was used to select two dates (one from 2019 and one from 2020) as the low flow cases. This process was done using the NWM operational analysis and assimilation data. Figure 3 displays the hydrographs for the reach where the low flow periods can be seen in 2019 and 2020.

For the high flows, there were fewer options to select therefore a different approach was taken. We calculated the return periods for floods based on the NWM retrospective data for the representative reach within the region. We calculated the return periods on data from 1980-2018 using the Gumbel Type 1 distribution:

$$Q_{rp} = -\log\left(-\log\left(1-\frac{1}{\mathrm{rp}}\right)\right)\cdot\sigma\cdot 0.7797\cdot\mu-(0.45\cdot\sigma)\,, \tag{5}$$

where Q_{rp} is the return period flow, rp is the return period in years, σ is the standard deviation of the dataset, and μ is the average of the dataset. Next, we evaluated the return periods against the NWM operational analysis and assimilation from late 2018 - 2020 to identify time periods where the flow exceeded return periods. We used the NWM operational product to evaluate return periods because these are the data that would hypothetically be used in actual situations for forecasting FIER. Another criterion for selection was finding dates where the data were reserved and not used for training the models but used for evaluation. We selected a date that exceeded a 50-year return period in 2019 as well as a separate date that exceeded a 5-year return period as flooding case studies to evaluate FIER predictions. We selected these events in order to have an extreme flooding event and a more common flooding case.

https://doi.org/10.5194/egusphere-2024-3491
Preprint. Discussion started: 15 November 2024

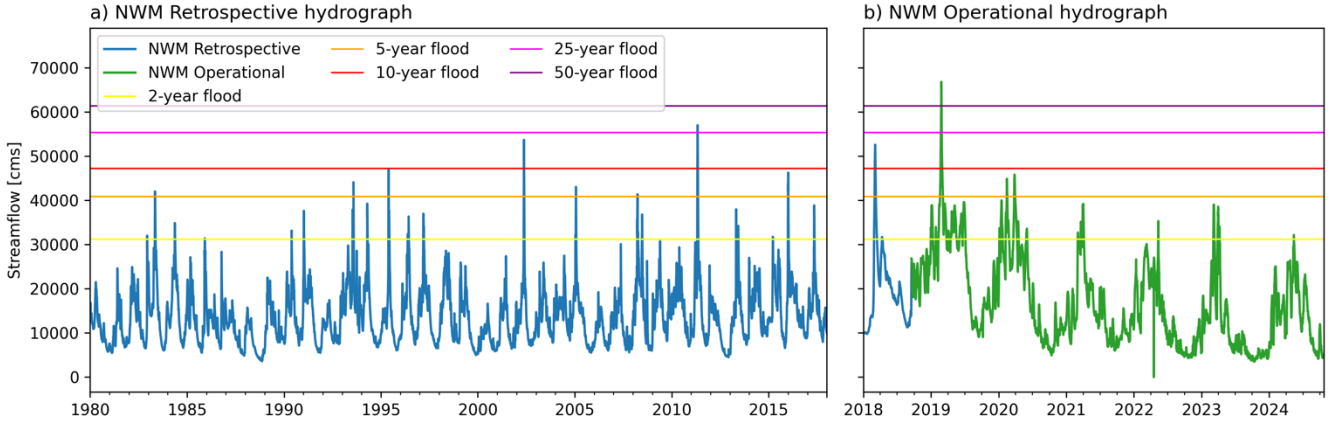

Figure 3: Streamflow hydrograph from the National Water Model (NWM) for the representative reach showing (a) retrospective simulations from 1980-2017 and (b) operational simulations from the analysis_assim run from 2018-2024. Horizontal lines indicate the 2-, 5-, 10-, 25-, and 50-year flood recurrence interval discharge values for the stream reach.

We ran FIER with streamflow data from a nowcast from the analysis and assimilation, 7-day medium-range forecast, and with a 15-day long-range forecast from the NWM to evaluate how different forecast runs and time horizons affect the FIER outputs. Since NWM produces sub-daily streamflow predictions, we averaged the streamflow values for the prediction date to use as inputs into FIER. The medium-range and long-range NWM streamflow predictions have multiple ensemble runs, so we averaged these across the different ensembles. The medium-range and long-range streamflow predictions have multiple initialization times; we used the 00Z initialization for the forecasts to have a single forecast when calculating the streamflow values for the FIER extent predictions. We used the same statistics to evaluate the outputs from FIER for each of these use cases.

4 Results

4.1 Statistical Analysis

The experimental design aimed to assess the feasibility of applying the FIER method over larger geographic scales by segmenting the area of interest (AOI) into multiple smaller watersheds and then mosaicking the results together. An analysis of the REOF process and regressions are provided in Appendix A. Here we focus on comparing the results of the mosaicked process to running FIER over a larger baseline area. Figure 4 displays the average error metrics and how they vary with buffer sizes. First, applying FIER to multiple watersheds and then mosaicking the results does not lead to poor performance compared to running FIER over the baseline AOI. When considering the original FIER outputs (green lines), Fig. 4 shows that the performance of the mosaicked results perform better than the baseline when the buffer size is smaller (0-10 km). When the buffer size is larger (20-50 km) then the error metrics of the mosaicked results begin to trend more closely aligned

https://doi.org/10.5194/egusphere-2024-3491
Preprint. Discussion started: 15 November 2024

to the baseline however are not that much lower than the SSIM metric at the lower buffer sizes. This is true for the SSIM, RMSE, and MAE metrics. For the RRMSE metric, the mosaicked results show higher errors from the original FIER outputs (no correction applied) compared to the baseline outputs but are closer to the baseline for the 1 and 2 km buffer experiments. When considering the post-processed outputs (blue lines), the mosaicked results perform better than the baseline for all the error metrics except for RRMSE. This is particularly notable for the SSIM metric, indicating that the post-processing applied to the mosaicked outputs are able to better capture the spatial patterns of observed flood inundation more effectively than either the baseline FIER output with post-processing or original outputs.

A noteworthy observation is the increase in error metric values for the post-processed FIER outputs compared to the original outputs, particularly noticeable in the RMSE and RRMSE values (Fig. 4 blue lines compared to green lines in graphs b and c). Interestingly, the RMSE for the post-processed mosaicked results is much lower than that of the post-processed baseline output (blue lines in graph b). Moreover, this pattern of increasing error values is not present for MAE (graph d). RMSE and RRMSE gives more weight to larger errors, meaning these metrics are more sensitive to outliers than MAE. The results suggest that the post-processing reduces the absolute errors but introduces few larger errors than were present in the original outputs.

https://doi.org/10.5194/egusphere-2024-3491
Preprint. Discussion started: 15 November 2024

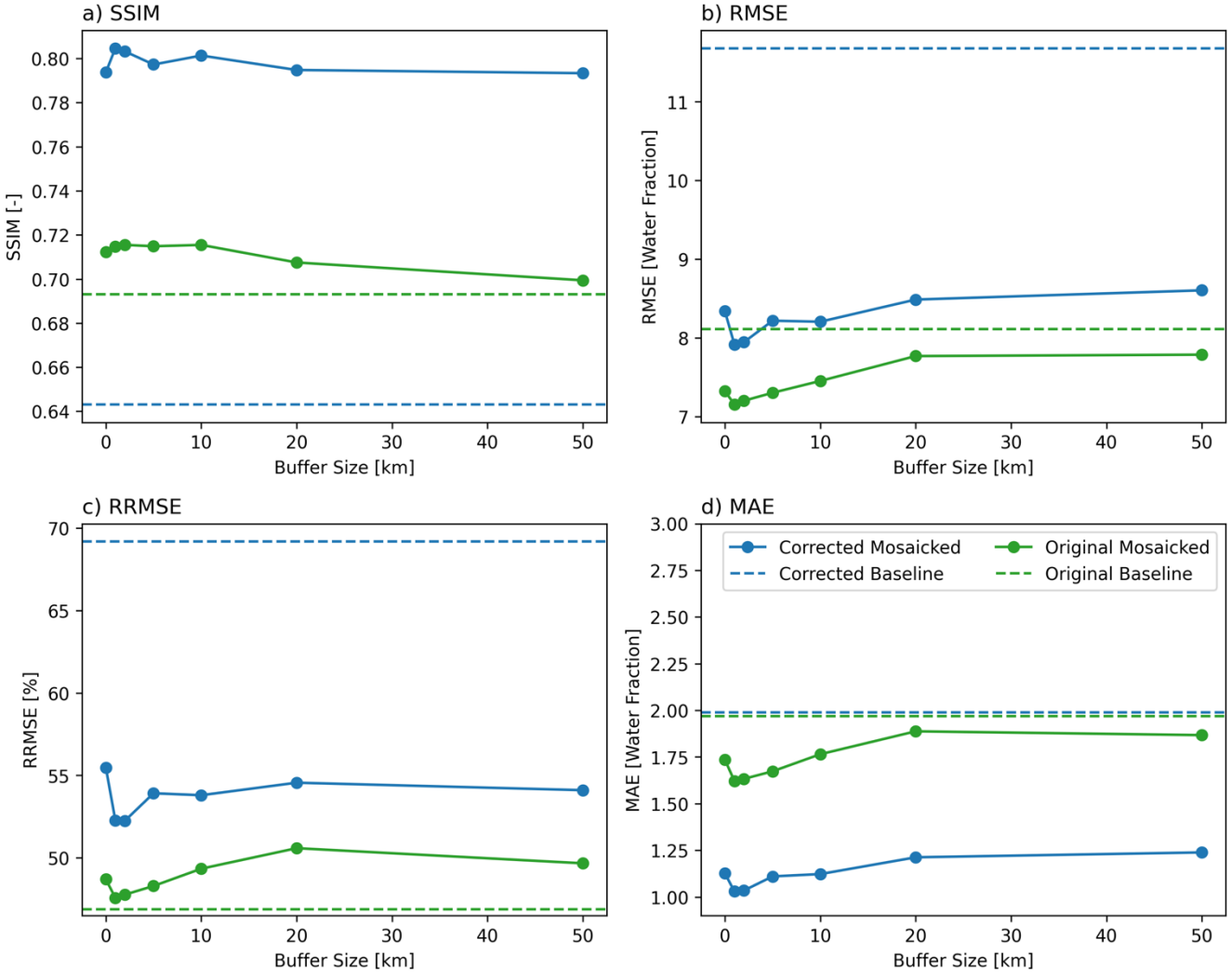

Figure 4: Graphs illustrating the impact of varying buffer sizes on the performance of the FIER method for flood inundation mapping, assessed using the areal average of four different metrics: (a) Structural Similarity Index Measure (SSIM), (b) Root Mean Squared Error (RMSE), (c) Relative Root Mean Squared Error (RRMSE), and (d) Absolute Error. The green lines represent the original FIER outputs, while the blue lines depict the corrected outputs after applying a CDF matching post-processing step. The dashed lines indicate the baseline performance metrics obtained from applying FIER to a single, larger AOI.

The other statistical analysis we performed was to compare the distributions of the errors. Figure 5 displays the CDF for the various error metrics and compares the baseline FIER predictions to the mosaicked FIER predictions with different buffer sizes. The CDF plots show that the original outputs (top row) have similar curve shapes aside from at the upper quantiles (0.8 - 1) where the mosaicked results for SSIM metric show more values with better performance compared to the baseline (black line). Conversely, the RMSE, RRMSE, and MAE curves show more values with greater errors compared to the baseline. The plots displaying the post-processed CDFs (bottom row) display a different pattern compared to the original

https://doi.org/10.5194/egusphere-2024-3491
Preprint. Discussion started: 15 November 2024

outputs. The SSIM curve for the mosaicked outputs displays better SSIM values compared to the baseline. However, the RMSE, RRMSE, and MAE CDF plots show that the post-processed mosaicked results have fewer values with less error (better performance) compared to the baseline for the lower quantiles (0 - 0.4) but have more values with higher errors (worse performance) at the upper quantiles (0.8 - 1) suggesting that the majority of errors for the post-processed results are due to large discrepancies with the observed. This supports the finding from comparing buffer sizes (Fig. 4) where the averaged RMSE metric worsens after the correction. The larger number of high error values can lead to higher RMSE and lower MAE errors because the RMSE metric is more sensitive to outliers than MAE.

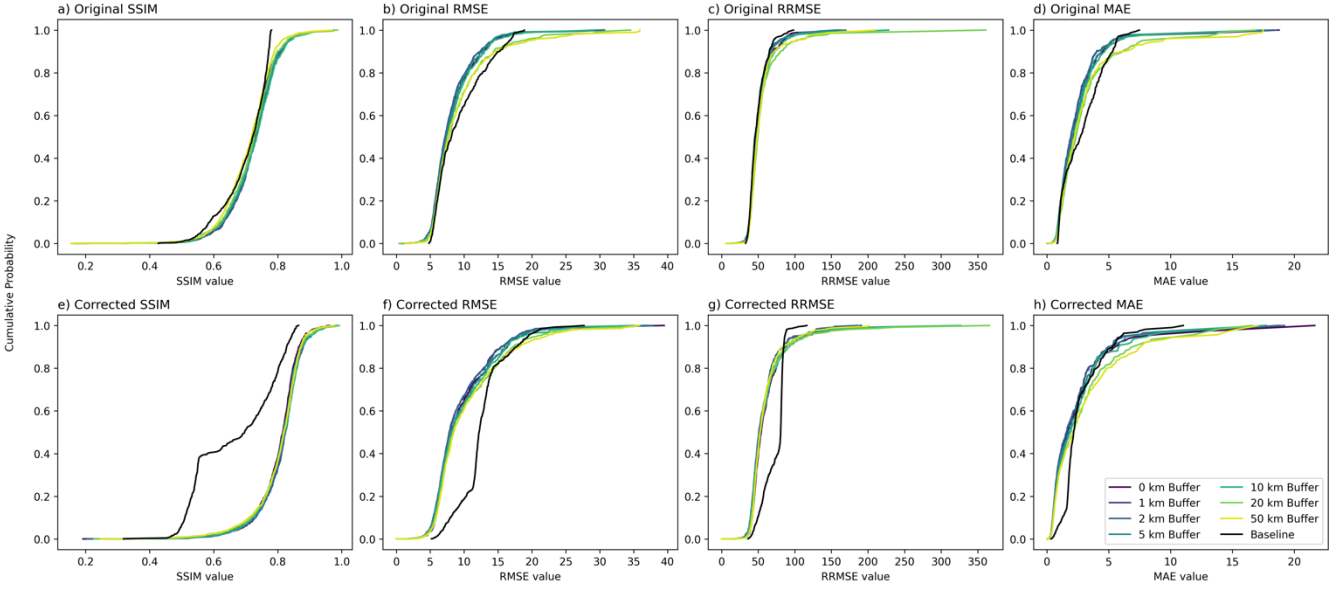

Figure 5: Cumulative distributions of different error metrics for the FIER spatial scaling experiments. The top row (a-d) shows the original FIER outputs, while the bottom row (e-h) shows the outputs after applying CDF matching as post-processing. Different colors represent varying buffer sizes used when delineating individual watersheds for the mosaicked FIER approach. The black line represents the baseline FIER run over the larger area. The metrics include: (a, e) SSIM, (b, f) RMSE, (c, g) RRMSE, and (d, h) MAE.

Table 1 provides the p-values from one-sided Kolmogorov-Smirnov tests, indicating whether the distributions from the various approaches are statistically different. The p-values from the Kolmogorov–Smirnov test reveal that there are significant differences between the baseline FIER and the mosaic approach across both the various error metrics and buffer sizes. In general, the buffer sizes of 20 and 50 km show that the mosaicked results are not statistically better (higher SSIM or lower RMSE, RRMSE, and MAE) than the baseline for the original outputs. Furthermore, the mosaicked results for buffer sizes of 0-10 km have significantly better performance only for the SSIM and RMSE. While the mosaic outputs have values less than the baseline for the MAE metric, this difference is not significant. Additionally, the mosaicked outputs have a higher RRMSE than the baseline.

https://doi.org/10.5194/egusphere-2024-3491
Preprint. Discussion started: 15 November 2024

For the corrected FIER outputs, all buffer sizes show statistically significant differences in SSIM compared to the baseline, indicating that by correcting the mosaicked outputs, the results are better able to capture the spatial distribution of flooding than using a single FIER process for a larger AOI. Furthermore, mosaic outputs show significantly better performance compared to the baseline AOI for the RMSE and MAE metrics. In particular, the p-values show that the buffer sizes 0-10 km are significantly less for RMSE, buffer size of 20 and 50 km are not significantly better. Whereas buffer sizes 0-20 km show statistically significant better performance compared to the baseline AOI for MAE and the buffer size of 50km is not significant. While the RRMSE metric was lower than the baseline for the corrected mosaicked results, the differences for all buffer sizes was not significant. This highlights that while post-processing aligns the spatial distribution of the flood predictions from FIER, it doesn't eliminate the inherent differences in the magnitude and spread of intensity-based errors between the two approaches. Overall, the Kolmogorov–Smirnov test results confirm that scaling FIER by mosaicking smaller watersheds produces statistically distinct error distributions, and that the buffer sizes 0-10 km are shown to result in more accurate predictions based on the error metrics tested compared to the baseline AOI.

Table 1: p-values from one-sided Kolmogorov-Smirnov tests comparing the distributions of evaluation metrics for FIER predictions with varying buffer sizes to the baseline FIER predictions. A lower p-value indicates a statistically significant difference between the distributions. Values denote significance at the 95% level are denoted with an asterisk (*), while values at the 99% level are denoted with double asterisks (**).

	Original				Corrected			
Buffer	**SSIM**	**RMSE**	**RRMSE**	**MAE**	**SSIM**	**RMSE**	**RRMSE**	**MAE**
0	0.0419*	0.0076**	0.9999	0.9878	0.0076**	0.0076**	0.6925	0.0076**
1	0.0241*	0.0074**	0.9813	0.1227	0.0074**	0.0025**	0.3697	0.0074**
2	0.0239*	0.0073**	0.9948	0.1865	0.0073**	0.0025**	0.3658	0.0073**
5	0.0234*	0.0072**	0.9973	0.1519	0.0072**	0.0044**	0.4869	0.0072**
10	0.0219*	0.0132*	1.0000	0.9826	0.0067**	0.0221**	0.6211	0.0089**
20	0.0876	0.1721	1.0000	0.9985	0.0064**	0.0648	0.6122	0.0749**
50	0.6267	0.2464	1.0000	0.9852	0.0121*	0.1276	0.4941	0.1087

These findings suggest that scaling the FIER method spatially by mosaicking results from smaller watersheds is a viable approach based on the error metrics tested. The mosaicked approach consistently achieves comparable or better spatial pattern accuracy (SSIM) than the baseline, and CDF matching further improves the accuracy of errors in water fraction estimates (RMSE and MAE) compared to the baseline. Furthermore, we found that the difference in mosaicked results error metrics are statistically significant. Larger buffer sizes (20 km and 50 km) do not show consistent improvements and may even lead to higher errors in some cases. This suggests that excessive buffering can blur the flood signal and reduce the accuracy of the predictions.

https://doi.org/10.5194/egusphere-2024-3491
Preprint. Discussion started: 15 November 2024

4.2 Case Studies

We performed the statistical analysis to understand the overall errors associated with running FIER over larger geographic scales using retrospective NWM streamflow as inputs, however, running FIER for actual flood extents necessitates using the operational NWM streamflow predictions for forecast predictions. We selected two dates with flooding and two dates with low flows then ran FIER for those time periods with only one buffer size to better understand how FIER does for extreme cases using the NWM operational data.

We selected which buffer size to use for the case study based on the statistical analysis that found a buffer size of 1 km or 2 km for mosaicked FIER outputs seems to be the most promising for operational use. While other buffer sizes show improvements in either SSIM or RMSE, we selected the 1 km buffer as it was found to strike a good balance between accurately capturing both the spatial extent and intensity of flooding when compared to the baseline. The corrected outputs demonstrate better error metric results (SSIM, RMSE, MAE) compared to the original outputs for the 1km buffer sizes which suggests that the CDF matching post-processing effectively reduces overall error in the flood inundation estimates therefore we used corrected output for this analysis. While we selected the 1km buffer size over a 2km buffer because the errors are slightly lower, these differences are marginal.

Figure 6 displays the results for running the mosaicked FIER process with the operational NWM predictions for the selected flood dates. Examining the 2019-02-25 flood event (top two rows), which exceeded the 50-year return period, FIER demonstrates consistent performance across nowcast, medium-range (7-day), and long-range (15-day) forecasts. The second row is zoomed into the baseline area to highlight more higher-resolution differences. Generally, it appears that the predictions capture the spatial dynamics of the flood, but the long-range prediction has a noticeably smaller extent than the nowcast or medium-range predictions. The 2020-02-15 flood event (bottom two rows), exceeding a 5-year return period, shows similar results where the forecasts are able to capture the extent of flooding, however, in this case the further the lead time for prediction the smaller the prediction of flood extents, suggesting more uncertainty with longer range forecasts. Table 2 tabulates the error metrics for each simulation compared to the observation. While the long-range forecast exhibits slightly higher RMSE compared to the nowcast and medium-range for the 2019-02-25 flood event, the differences are marginal, and all forecasts achieve SSIM values above 0.57, indicating reasonable agreement with the observed flood extent. This suggests that FIER can provide reliable flood inundation predictions even with extended lead times, allowing for proactive flood mitigation measures.

The 2020-02-15 flood event, exceeding the 5-year return period, showcases even better performance, particularly for the long-range forecast. This forecast achieves the highest SSIM of 0.67 and lowest RMSE 16.04 among all predictions, highlighting the potential of FIER for capturing more frequent flood events with high accuracy. The nowcast for this event, however, shows a slight decrease in performance compared to the forecasts. The degradation in performance for the forecasts compared to the retrospective FIER simulations is likely due to the errors in the NWM streamflow predictions over the extended lead times.

https://doi.org/10.5194/egusphere-2024-3491
Preprint. Discussion started: 15 November 2024

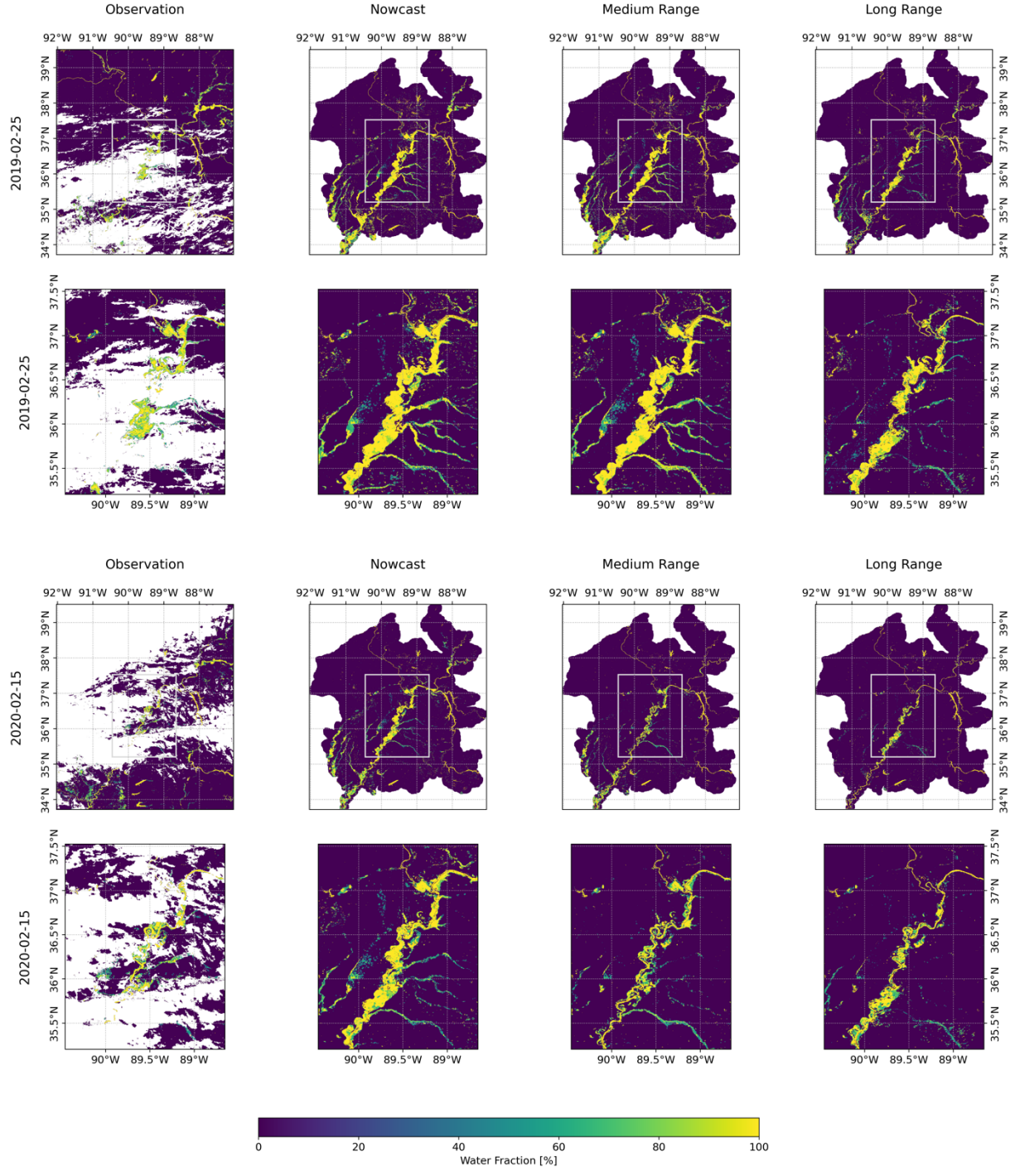

405 **Figure 6. Comparison of observed and FIER-predicted water fraction maps for the two selected flood events: 2019-02-25, the 50-year flood (top two rows), and 2020-02-15, the 5-year flood (bottom two rows) The lower rows are a zoomed view for the baseline area to highlight local differences in the predictions. Predictions use the nowcast, medium-range (7-day lead time) and long-range**

https://doi.org/10.5194/egusphere-2024-3491
Preprint. Discussion started: 15 November 2024

(15-day lead time) streamflow from the NWM. White areas are missing data due to clouds, cloud shadows and other poor-quality data.

Table 2: Performance statistics for the FIER-predicted water fraction maps for two flood events 2019-02-25, the 50-year flood, and 2020-02-15, the 5-year flood.

Date	Forecast	SSIM [-]	RMSE [Water fraction]	RRMSE [%]	MAE [Water fraction]
2019-02-25	Nowcast	0.5723	16.9233	78.482	3.9396
	Medium range	0.5766	17.2939	80.201	4.0435
	Long range	0.6664	16.2569	75.391	3.5162
2020-02-15	Nowcast	0.5414	18.4803	79.022	4.6667
	Medium range	0.6233	16.3844	70.060	3.6701
	Long range	0.6676	16.0370	68.575	3.4319

The evaluation of FIER performance during low flow periods, using operational NWM streamflow predictions and the selected 1 km buffered and corrected configuration, reveals consistent and accurate results. Figure 7 displays the results for running the mosaicked FIER process with the operational NWM predictions for the selected low-flow dates. Table 3 shows the resulting error statistics comparing the FIER mosaicked predictions with the observation for the two selected low-flow dates. For the 2019-09-29 low flow event, FIER exhibits high SSIM values (above 0.73) across all forecast ranges, indicating strong agreement with the observed low flow conditions. The long-range (15-day) forecast demonstrates the lowest RMSE (8.53) and MAE (0.89), suggesting that FIER can effectively capture low flow dynamics even with extended lead times. This capability is particularly valuable for water resource management applications, such as drought monitoring and water allocation planning. Similarly, the 2020-10-21 low flow event shows consistent performance across all forecast ranges, with SSIM values exceeding 0.73. Again, the long-range forecast achieves the lowest RMSE (8.01) and MAE (0.79), reinforcing the ability of FIER to accurately predict low flow conditions with extended lead times. The visual comparison of the FIER-predicted water fraction maps (Fig. 7) with the observed data further supports these findings. The FIER predictions closely match the observed low flow extents, particularly for the nowcast and medium-range forecasts. The FIER outputs using the streamflow forecasts, while still capturing the general low flow patterns, show some minor deviations, likely attributed to the inherent uncertainties in the model streamflow predictions.

These results highlight the potential of the scaled FIER method for operational low flow forecasting. The consistent performance across different forecast ranges, coupled with the high SSIM values and low error metrics, demonstrates the capability of FIER to provide reliable and accurate low flow predictions. This information can be crucial for informing water management decisions, mitigating drought impacts, and ensuring sustainable water resource allocation during periods of low flow.

https://doi.org/10.5194/egusphere-2024-3491
Preprint. Discussion started: 15 November 2024

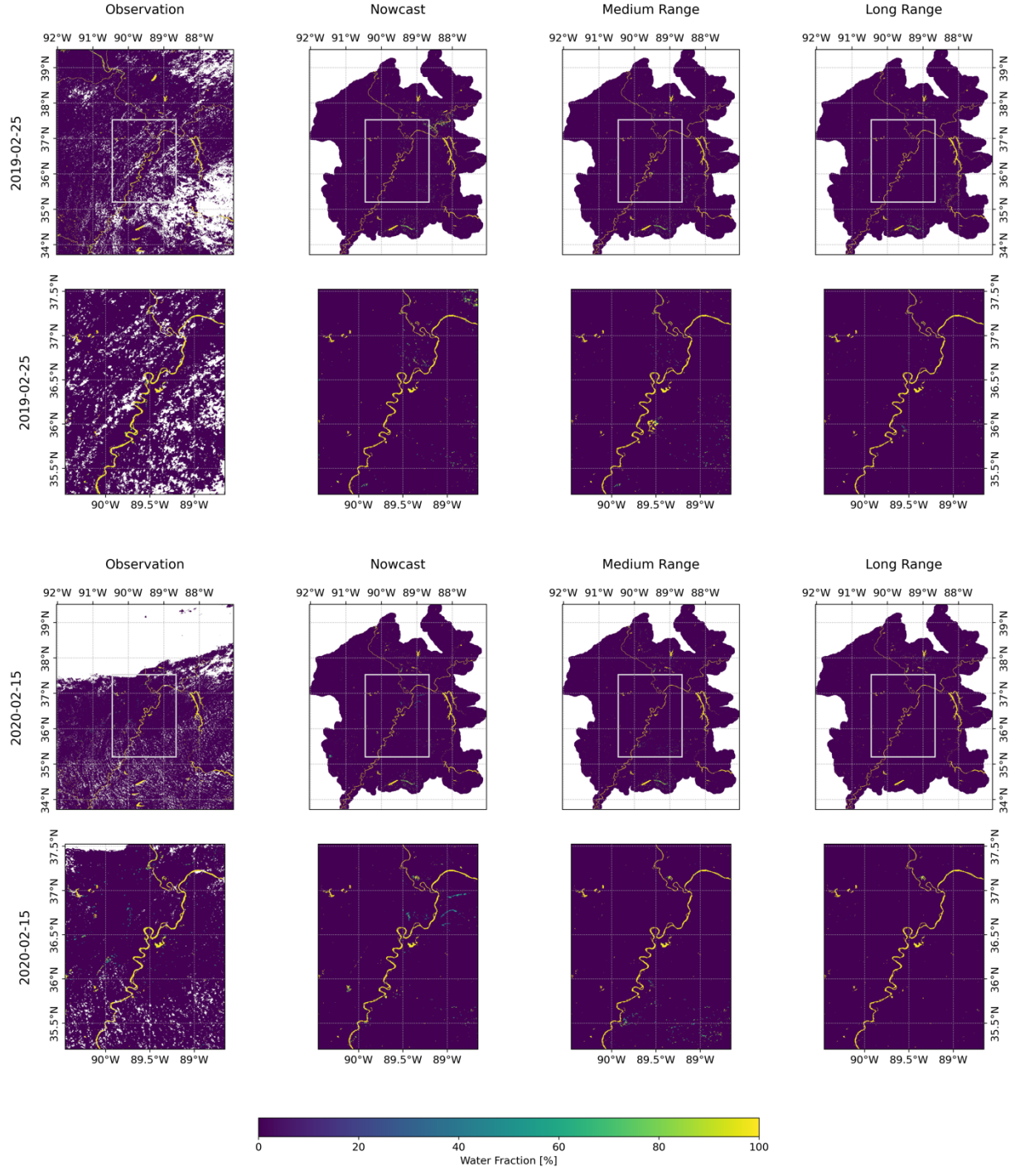

435 **Figure 7. Same as Fig. 6 except for the two selected low-flow dates: (top two rows) 2019-09-29 and (bottom two rows) 2020-10-21. Predictions use the nowcast, medium-range (7-day lead time) and long-range (15-day lead time) streamflow from the National Water Model. White areas are missing data.**

https://doi.org/10.5194/egusphere-2024-3491
Preprint. Discussion started: 15 November 2024

Table 3: Performance statistics for the FIER-predicted water fraction maps for two selected low-flow dates: 2019-09-29 and 2020-10-21.

Date	Forecast	SSIM [-]	RMSE [Water fraction]	RRMSE [%]	MAE [Water fraction]
2019-09-29	Nowcast	0.7381	9.8846	68.336	1.2012
	Medium range	0.7580	8.6568	59.848	0.9179
	Long range	0.7688	8.5340	58.998	0.8879
2020-10-21	Nowcast	0.7374	8.7395	61.268	0.9843
	Medium range	0.7394	8.7107	61.067	0.9571
	Long range	0.7713	8.0128	56.174	0.7921

5 Discussion

5.1 Advantages and Limitations of the Watershed-Based Approach

Scaling the FIER method to larger geographic extents necessitates breaking the larger AOI into subunits. Hydrological regimes, topography, and flood characteristics vary significantly across different geographical locations, requiring regionally tailored implementations for accurate predictions. Furthermore, FIER is a data driven method meaning that the method is dependent on the data inputs and the patterns it can extract from the data. Using watersheds as the fundamental unit offers several advantages. Primarily, watersheds inherently delineate areas with interconnected hydrological regimes, ensuring that flood signals within each unit are driven by a common set of forcing factors. This allows for the development of regionally tailored FIER models that better capture the unique flood characteristics of each watershed. Additionally, by dividing a large area into smaller watersheds, the computational burden of FIER can be significantly reduced, facilitating parallel processing and enabling the application over extensive regions where limitations of computer resources can inhibit applying one FIER model.

Despite these advantages, the watershed-based approach presents certain limitations. One challenge lies in the potential for discontinuities at watershed boundaries when mosaicking individual FIER predictions. Abrupt transitions in predicted water fractions can arise due to variations in model parameters or data availability across watersheds. We showed that implementing the buffered approach around each watershed during the FIER fitting process mitigates this issue (Fig. 4) by incorporating information from neighboring areas and smoothing the flood signal across boundaries. However, the optimal buffer size is likely to vary depending on watershed characteristics and requires careful consideration. We found that selecting an excessively large buffer size risks blurring the flood signal and reducing the accuracy of predictions. More

https://doi.org/10.5194/egusphere-2024-3491
Preprint. Discussion started: 15 November 2024

investigation is needed into what factors contribute to varying accuracy, particularly watershed characteristics such as size, topography, land cover, meteorology/climatology and flooding events.

Furthermore, the choice of watershed scale (i.e. HUC8 vs HUC12) has the potential to influence the performance of the scaled FIER model. Utilizing smaller, more numerous watersheds allows for finer spatial resolution and can potentially capture localized flood dynamics more effectively. However, using more watersheds comes at the cost of increased computational complexity and the potential for greater boundary discontinuities. Conversely, larger watersheds simplify the mosaicking process but may omit fine-grained flood signals and fail to capture fine-scale variations in inundation extent. Ultimately, the optimal watershed scale and buffer size are likely to be site-specific and require careful evaluation based on the hydrological characteristics, computational resources, and desired level of spatial detail for the application. For this study we only used the HUC8 watershed scale for comparing how FIER performs when mosaicking; using different watersheds scales was out of scope for this work but is a topic for future research.

5.2 Implications for Large-Scale Flood Inundation Forecasting

The results from this study show that FIER can be successfully implemented over large areas using a mosaicking approach. The successful scaling of the FIER method holds significant implications for operational flood inundation forecasting at regional and continental scales. FIER's data-driven nature and computational efficiency make it particularly well-suited for large-scale applications where traditional hydrodynamic models are often computationally prohibitive or require extensive data inputs. By leveraging readily available satellite imagery and streamflow forecasts from hydrological models, like the NWM, FIER can provide rapid and accurate flood inundation predictions without the need for a complex modeling framework, calibration, or high-resolution topographic data. This data independence makes FIER a powerful tool for forecasting floods in data-scarce regions or ungauged basins, expanding the reach of flood inundation forecasting services to areas previously underserved regions (Chang et al., 2023; Do et al., in review).

The scaled FIER method offers a valuable resource for a wide range of applications related to flood risk assessment, disaster preparedness, and water resource management. By providing timely and accurate flood inundation forecasts for events, FIER can support the development of effective early warning systems, enabling communities to prepare for and mitigate the impacts of flooding. In the context of water resource management, FIER can contribute to simulating flood responses to changes in hydrologic conditions which can inform flood risk assessments and guide long-term land-use planning decisions, optimizing reservoir building and operations (Do et al., in review), assessing the effectiveness of flood control measures, and evaluating the impacts of climate change and human activities on flood regimes. Furthermore, FIER's ability to generate flood inundation maps from historical and even future long-term projected data can provide extents for specific return-periods which are vital with regards to climate change and planning (Wing et al., 2024). The scalability and computational efficiency of FIER hold promise to support large-scale flood inundation forecasting, enabling a more proactive and data-driven approach to flood risk management.

https://doi.org/10.5194/egusphere-2024-3491
Preprint. Discussion started: 15 November 2024

5.3 Caveats and Limitations

The watershed-based approach for scaling FIER, while promising, presents several limitations that warrant further investigation. The use of buffer zones, while mitigating abrupt transitions at watershed boundaries, may introduce artificial delineations that may not accurately represent the complex hydrological connectivity of real-world systems. For instance, in areas with complex topography or where floodwaters overtop watershed divides, the buffer zones may lead to inaccuracies in the mosaicked flood predictions. As demonstrated in the statistical analysis, buffer sizes between 1-10 km showed the most promising results, but further research is needed to optimize buffer zone selection based on specific watershed characteristics and flood dynamics. Similarly, the choice of watershed scale presents a trade-off between spatial resolution and computational complexity. While smaller watersheds offer finer detail, they increase the potential for boundary discontinuities and computational burden. Conversely, larger watersheds simplify mosaicking but risks over smoothing the flood signal and missing localized flood events. The optimal scale is likely to be site-specific, requiring careful consideration of the desired level of detail and available computational resources.

Furthermore, the current FIER implementation's reliance solely on streamflow data as the hydrological driver, in this case NWM streamflow outputs. This limits its applicability in data-scarce regions or where streamflow observations are unreliable. Other large scale model data (e.g. GEOGLOWS, Hales et al., 2022) can be used and tested to understand how sensitive the approach is to input streamflow particularly for data-scare regions across the globe. Additionally, the focus on streamflow-driven flooding may not adequately represent other flood types, such as coastal flooding, flash floods, or pluvial flooding, which are not directly tied to streamflow variations. Expanding the framework to incorporate other hydrological variables, such as precipitation, soil moisture, and antecedent conditions, could enhance its robustness and broaden its applicability. While the use of VIIRS data provides daily observations, data gaps due to cloud cover remain a challenge. Integrating data from multiple satellite sensors, such as SAR and optical imagery could further improve the temporal density and quality of the input data (Markert et al., 2018). Finally, it is crucial to acknowledge that the performance of the scaled FIER model may vary across different geographic regions with diverse hydrological regimes and flood characteristics. The location used in this study along the Mississippi River is humid with varying land cover types compared to the Western US which is much drier but also experiences flooding where FIER may be applicable. Further validation and testing in various environments are necessary to assess its generalizability and transferability beyond the study areas examined in this research.

5.4 Future Work

While this study demonstrates the potential of the scaled FIER method for large-scale flood inundation forecasting, several avenues for future research can further enhance its accuracy and applicability. First, exploring alternative regression methodologies between streamflow and the FIER-derived temporal patterns (RTPCs) could improve the model's ability to capture complex flood dynamics. Other studies (e.g. Chang et al., 2023, Rostami, et al. in review) have used dense neural networks (DNN) to create the forecasts in the FIER framework. Incorporating non-linear regression techniques, like DNN, in

https://doi.org/10.5194/egusphere-2024-3491
Preprint. Discussion started: 15 November 2024

a scalable manner and additional hydrological variables, such as precipitation and soil moisture, may enhance the model's predictive capabilities. Second, FIER is data driven and by using optical satellite imagery from VIIRS may lead to data gaps for floods which often occur coincidentally with cloud cover (Markert et al., 2020) which results in FIER not capturing the signal. Data fusion methods (e.g. (Markert et al., 2024a) may provide opportunities to capture additional flood observations and yield better results for flood periods. A systematic analysis of the relationship between buffer size and watershed characteristics is crucial for optimizing the mosaicking process. By examining factors like watershed size, shape, topography, and land cover, we can develop guidelines for selecting appropriate buffer sizes for different regions, minimizing boundary discontinuities while preserving the accuracy of individual FIER predictions. Additionally, it was mentioned that only one watershed scale was tested (HUC8) and different sizes of watersheds need to be tested to understand how the FIER results will be affected by watershed sizes. This can lead to a hybrid approach where buffer size and watershed scale for running FIER can be data-driven and yield better results over large areas. Finally, to further enhance computational efficiency, masking out watersheds with historically limited flooding from the analysis can significantly reduce processing time. This targeted approach focuses computational resources on areas most prone to flooding, enabling more efficient application of FIER over large geographic extent.

6 Conclusion

This study aimed to address the critical need for efficient and accurate large-scale flood inundation forecasting by applying the FIER method, a data-driven technique previously demonstrated at smaller scales, over large areas. Recognizing the limitations of traditional hydrodynamic models and the need for a computationally efficient approach for event-based forecasting, we investigated the feasibility of using a watershed-based approach to scale FIER, leveraging the inherent hydrological connectivity of watersheds and then mosaicking results to create a single flood map for a given simulation. Our analysis focused on flood-prone regions in the United States, the Upper Mississippi Alluvial Plain, where flooding occurs often.

The results demonstrate the effectiveness of the watershed-based approach for scaling FIER. Statistical analysis of the mosaicked FIER predictions, using retrospective NWM streamflow data, revealed that buffer sizes of 1-10 km achieved the best balance between accurately capturing the spatial extent (SSIM) and intensity (RMSE) of flooding. The average SSIM metric ranged from 0.714 to 0.715 for the original FIER outputs and 0.797 to 0.804 for the corrected outputs. Whereas the average RMSE metric ranged from 7.15 to 7.45 for the original FIER outputs and from 7.91 to 8.21 percent for the corrected outputs. Notably, the corrected FIER outputs, using a CDF matching post-processing technique, consistently showed better SSIM error values compared to the original outputs but higher RMSE and lower MAE, suggesting the overall error was reduced but also introduced larger errors. Overall, the correction improves the predictions and yields significantly better error metrics compared to a baseline for the 1-10 km buffer sizes. Case studies using operational NWM streamflow forecasts for specific flood and low flow events further validated the performance of the scaled FIER method. The 1 km buffered and

https://doi.org/10.5194/egusphere-2024-3491
Preprint. Discussion started: 15 November 2024

corrected FIER outputs were used for the case study and coupled with NWM forecasts with varying forecast lead times. These flood extent predictions accurately forecasted both the extent of inundation, achieving SSIM values above 0.54-0.66 for flood events and above 0.73 for low flow events.

The watershed-based FIER approach offers several advantages, including the ability to capture regional flood characteristics and the ability to set up and run from compute perspective without the need of prohibitively expensive hardware resources. However, limitations such as boundary effects, sensitivity to watershed scale, and reliance on streamflow data require further investigation. Future research should focus on optimizing buffer zone selection based on watershed characteristics, exploring alternative regression methodologies, incorporating additional hydrological variables, and expanding the framework to encompass non-fluvial flood processes. These advancements will further enhance the scalability, accuracy, and applicability of FIER for large-scale flood inundation forecasting, enabling more effective flood risk management and water resource planning.

Appendix A: FIER fitting statistics

We performed additional analysis to investigate and highlight the results of the fitting process between the REOF and hydrologic data. We separated the analysis into the baseline area and the full area with the different watersheds.

For the baseline area, we found that the first three modes of spatio-temporal patterns were significant and account for about 93% of the total variance of the VIIRS water fraction image time series. Hereafter, the first modes of the RSM or RTPC will be called RSM-01 or RTPC-01, respectively with the second mode of RSM or RTPC will be called RSM-02 or RTPC-02, respectively, and so forth.

Figure A1 displays the results of the REOF and fitting for the baseline area. The top row displays the first three RSMs, revealing distinct spatial flooding patterns captured by VIIRS water fraction data. RSM-01 exhibits a widespread pattern encompassing the main stem of the Mississippi River and its tributaries, suggesting a dominant mode of flooding associated with high flows in the main channel. RSM-02, highlights localized flooding patterns in the southeastern portion of the basin, potentially indicating areas susceptible to backwater effects or tributary flooding. RSM-03 shows a more dispersed pattern with both positive and negative values, suggesting a complex mode of flooding that may be influenced by a combination of factors. The middle row in Fig. A1 presents the time series of the corresponding RTPCs and normalized NWM streamflow for the representative reach. The close alignment between the RTPC fluctuations and streamflow variations, particularly for RTPC-02, indicates a strong correlation between these temporal patterns and the hydrological driver. The three RTCPs have a Pearson's R correlation coefficient of 0.7342, 0.8722, and 0.7615 for modes RTPC-01, RTPC-02, and RTPC-03, respectively. This correlation between the RTCPs and streamflow is further quantified in the bottom row, which shows scatter plots of the RTPCs against normalized NWM streamflow, along with the fitted regression models. The high NSE values (0.61, 0.77, and 0.63) for the three fitted models confirm the strong statistical relationships established between the flood patterns and streamflow, demonstrating the effectiveness of the regression models in capturing these relationships.

https://doi.org/10.5194/egusphere-2024-3491
Preprint. Discussion started: 15 November 2024

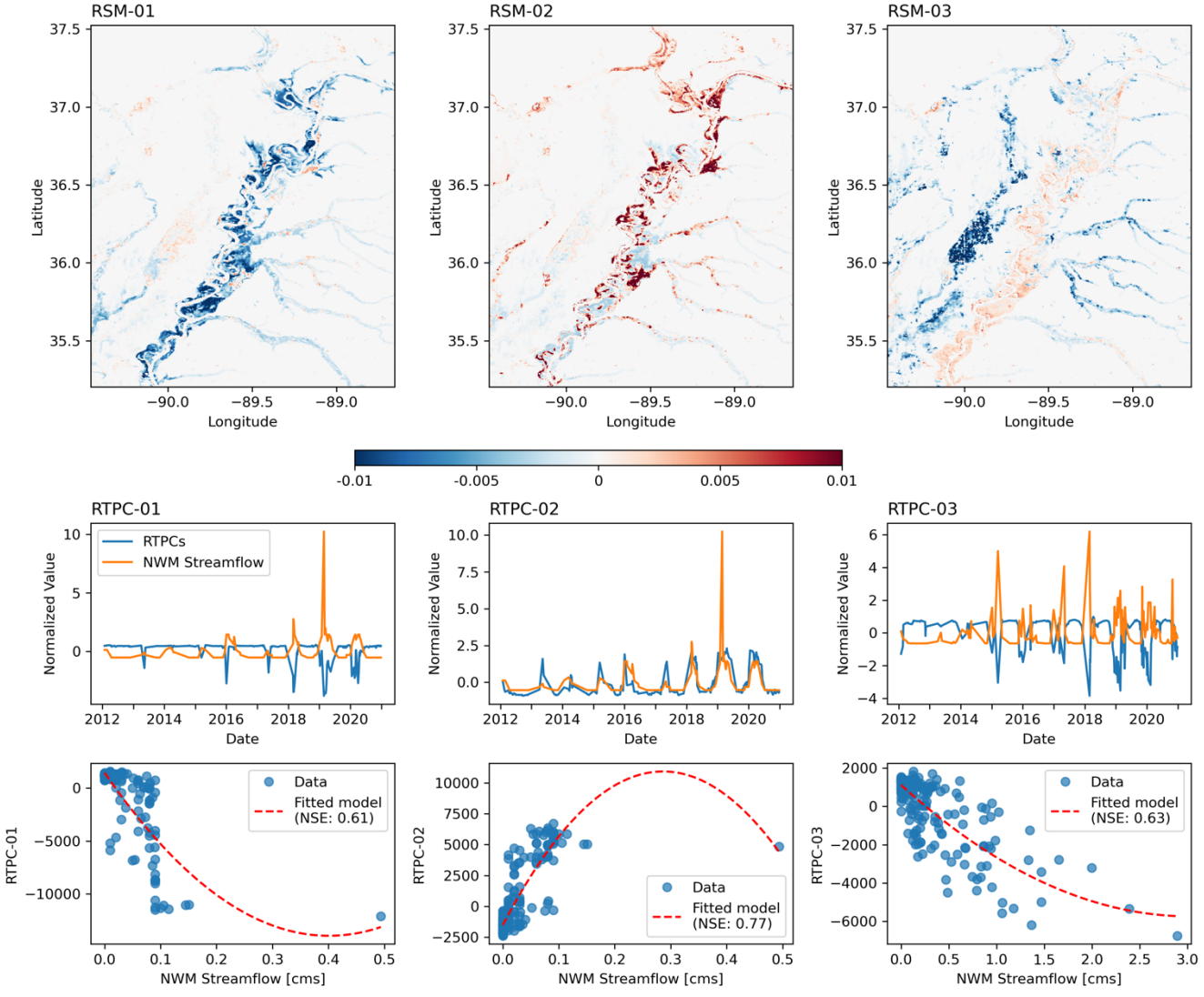

590 **Figure A1: Spatiotemporal patterns and regression models for the baseline area. (Top) The first three Rotated Spatial Modes (RSMs) derived from REOF analysis of VIIRS water fraction data. Red colors indicate positive values, while blue colors indicate negative values. (Middle) Time series of the corresponding Rotated Temporal Principal Components (RTPCs) (blue) and normalized NWM streamflow (orange) for the representative reach. (Bottom) Scatter plots of the RTPCs against normalized NWM streamflow, along with the fitted regression models (red dashed lines) and their corresponding Nash-Sutcliffe Efficiency**
595 **(NSE) values.**

Figure A2 provides a view of how the performance of the scaled FIER method varies across different buffer sizes and watersheds. Given that there is so much data across the different REOF and regression processes, Fig. A2 summarizes the number of RSMs (left column), correlation between RTCPs and streamflow (middle column) and NSE from the fitted model
600 (right column) for each watershed. Table A1 also provides the mean and stand deviation in parenthesis for each of the

https://doi.org/10.5194/egusphere-2024-3491
Preprint. Discussion started: 15 November 2024

metrics across all watersheds. Examining the number of significant RSMs, we observe a general trend of an increasing number of significant RSMs with larger buffer sizes. This suggests that incorporating information from neighboring watersheds through buffering enhances the ability of REOF analysis to capture distinct flood patterns. However, the average Pearson's correlation coefficient between RTPCs and streamflow remains relatively consistent across buffer sizes, ranging from an average of 0.727 to 0.765. This indicates that the strength of the relationship between flood patterns and streamflow is not significantly affected by the buffer size. Interestingly, the average NSE of the fitted regression models shows a more nuanced pattern. While smaller buffer sizes (0-2 km) exhibit relatively lower NSE values, indicating moderate model performance, the NSE gradually increases with larger buffer sizes, peaking at 0.616 for the 50 km buffer. This suggests that incorporating broader spatial context through larger buffer zones can improve the predictive capability of the regression models. However, it's important to note that the standard deviation of NSE also varies with buffer sizes. Overall, the analysis suggests that while the number of significant modes and the strength of the correlation between flood patterns and streamflow are not significantly impacted by buffer size, larger buffer zones can potentially enhance the predictive accuracy of the regression models. However, the increased variability in model performance with larger buffer sizes necessitates a careful consideration of the trade-offs between model complexity and accuracy when selecting the optimal buffer size for a given application.

Table A1: Summary statistics of REOF analysis and regression model performance for varying buffer sizes. The table shows the range of significant modes, average Pearson's correlation coefficient, and average NSE for each buffer size, with standard deviations in parentheses.

Buffer size	Range of Significant RSMs	Avg Pearson's R	Avg fit NSE
0 km	1 - 8	0.727 (0.038)	0.587 (0.060)
1 km	1 - 8	0.728 (0.039)	0.586 (0.063)
2 km	1 - 8	0.732 (0.037)	0.594 (0.070)
5 km	1 - 8	0.741 (0.041)	0.611 (0.070)
10 km	1 - 8	0.742 (0.032)	0.599 (0.052)
20 km	2 - 10	0.745 (0.037)	0.602 (0.058)
50 km	1 - 11	0.765 (0.029)	0.616 (0.049)

https://doi.org/10.5194/egusphere-2024-3491
Preprint. Discussion started: 15 November 2024

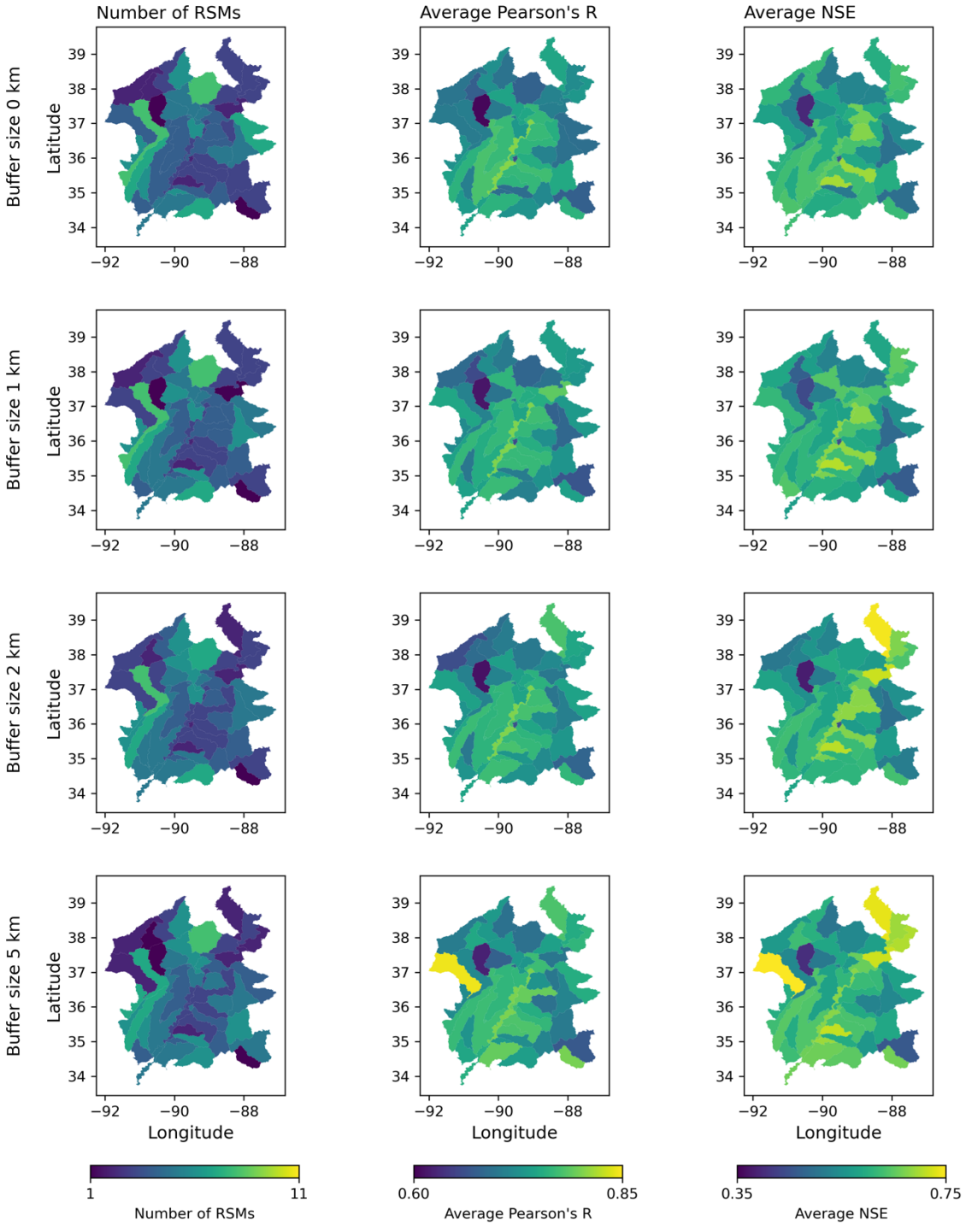

Figure A2: Spatial distribution of FIER model performance metrics for varying buffer sizes. The figure displays maps showing (left) the number of significant RSMs identified by the Monte Carlo test, (middle) the average Pearson's correlation coefficient

https://doi.org/10.5194/egusphere-2024-3491
Preprint. Discussion started: 15 November 2024

between the RTPCs and streamflow, and (right) the average Nash-Sutcliffe Efficiency (NSE) of the fitted regression models for each watershed, across different buffer sizes (0 km, 1 km, 2 km, 5 km).

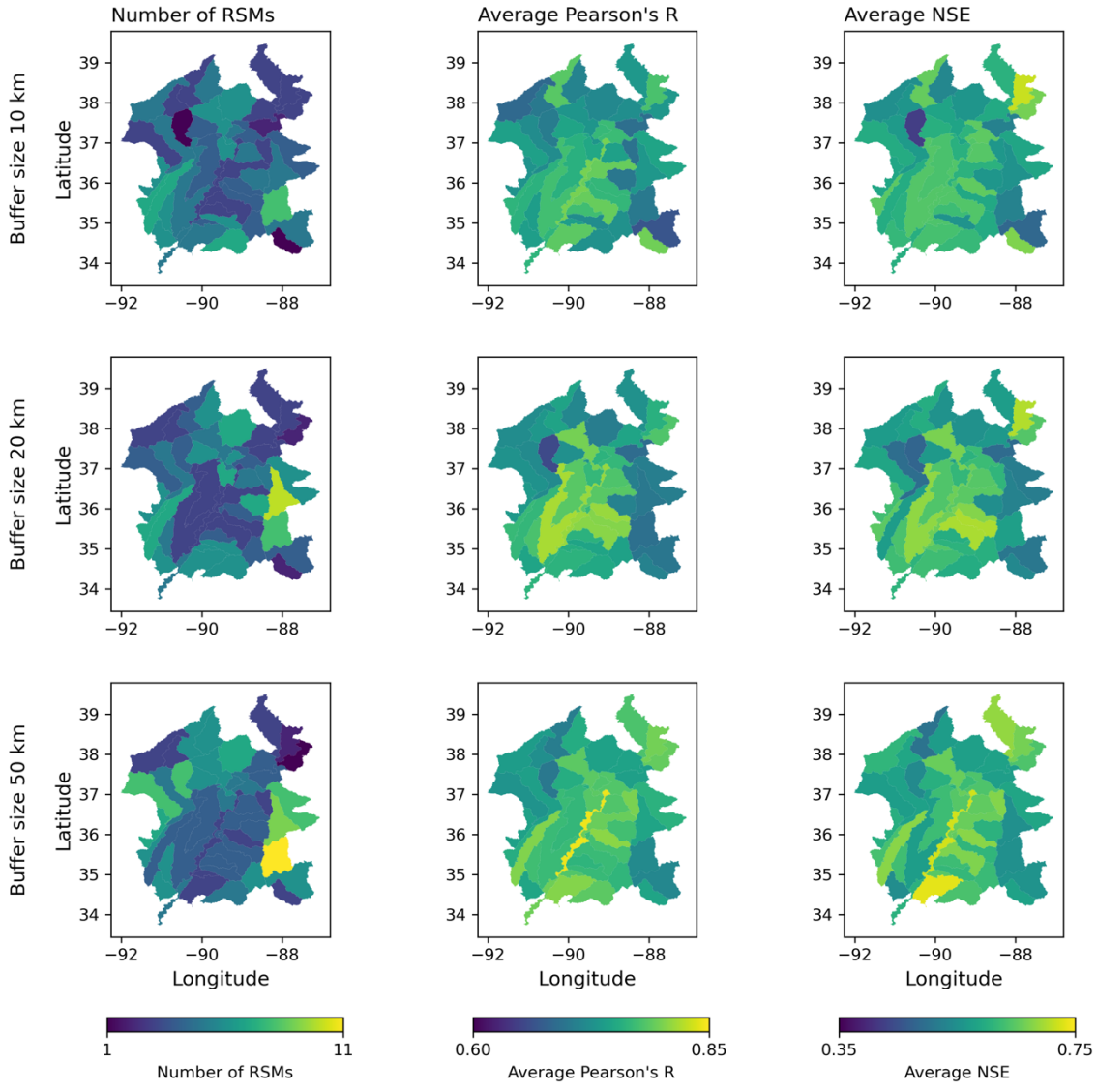

Figure A2 (continued): Same as Fig. A2 but showing for the buffer sizes 10 km, 20 km, and 50 km

Code availability

The software/scripts used in this study for data processing, analysis and figure generation are publicly available under the open-source Apache 2.0 license. The source code used can be accessed at https://github.com/KMarkert/phd-fier-scaling

https://doi.org/10.5194/egusphere-2024-3491
Preprint. Discussion started: 15 November 2024

(accessed on 7 Nov 2024). Developer: K.N.M.; year first available: 2024; license: Apache 2.0; programming language: Python.

Data availability

The data used in the study are openly available online. The VIIRS water fraction data can be accessed from the AWS Registry of Open Data, specifically the NOAA Joint Polar Satellite System (JPSS) cloud storage bucket (https://registry.opendata.aws/noaa-jpss/). We processed and stored the VIIRS water fraction data for North America publicly on Earth Engine with the following collection ID: "projects/byu-hydroinformatics-gee/assets/noaa_jpss_floods", we make no explicit guarantees to maintaining the collection on Earth Engine and the NOAA source should be considered the authoritative source. The NWM retrospective data can be accessed through the AWS Registry of Open Data from the NOAA National Water Model CONUS Retrospective Dataset (https://registry.opendata.aws/nwm-archive/). The operational NWM data can be accessed via the Google Cloud Public Dataset on BigQuery (https://goo.gle/nwm-on-bq).

Author contribution

Conceptualization, K.N.M., H.L, G.P.W., E.J.N. and D.P.A.; methodology, K.N.M.; software, K.N.M.; validation, K.N.M.; visualization, K.N.M., G.P.W, and H.L.; supervision: G.P.W., E.J.N., H.L., D.P.A. and R.E.G.; writing—original draft preparation, K.N.M., G.P.W., E.J.N., H.L. and D.P.A.; writing—review and editing, K.N.M., G.P.W., E.J.N., H.L., D.P.A. R.E.G. and F.J.M.; All authors have read and agreed to the published version of the manuscript.

Competing interests

K.N.M. is employed by Google; the methods presented use generally available Google technologies. D.P.A. is a member of the editorial board of the Environmental Modelling & Software journal. The other authors declare no conflicts of interest.

Acknowledgements

The authors would like to thank the data providers, particularly the National Oceanic and Atmospheric Administration (NOAA) Open Data Dissemination (NODD) Program for providing the JPSS VIIRS data and NWM data freely available for use. We would like to thank Google Open Datasets Program for publicly hosting the operational NWM on BigQuery and to the Google Earth Engine team for the use of the Earth Engine platform under the non-commercial terms of service for research. Gemini, a generative AI tool developed by Google, was used during manuscript editing to help improve clarity and proper grammar.

https://doi.org/10.5194/egusphere-2024-3491
Preprint. Discussion started: 15 November 2024

References

Bates, P. D., Pappenberger, F., and Romanowicz, R. J.: Uncertainty in Flood Inundation Modelling, in: Applied Uncertainty Analysis for Flood Risk Management, IMPERIAL COLLEGE PRESS, 232–269, https://doi.org/10.1142/9781848162716_0010, 2014.

Ben-Haim, Z., Anisimov, V., Yonas, A., Gulshan, V., Shafi, Y., Hoyer, S., and Nevo, S.: Inundation Modeling in Data Scarce Regions, https://doi.org/10.48550/arXiv.1910.05006, 30 October 2019.

Chang, C. H., Lee, H., Kim, D., Hwang, E., Hossain, F., Chishtie, F., Jayasinghe, S., and Basnayake, S.: Hindcast and forecast of daily inundation extents using satellite SAR and altimetry data with rotated empirical orthogonal function analysis: Case study in Tonle Sap Lake Floodplain, Remote Sensing of Environment, 241, 111732, https://doi.org/10.1016/J.RSE.2020.111732, 2020.

Chang, C.-H., Lee, H., Do, S. K., Du, T. L. T., Markert, K., Hossain, F., Ahmad, S. K., Piman, T., Meechaiya, C., Bui, D. D., Bolten, J. D., Hwang, E., and Jung, H. C.: Operational forecasting inundation extents using REOF analysis (FIER) over lower Mekong and its potential economic impact on agriculture, Environmental Modelling & Software, 162, 105643, https://doi.org/10.1016/j.envsoft.2023.105643, 2023.

Cosgrove, B., Gochis, D., Flowers, T., Dugger, A., Ogden, F., Graziano, T., Clark, E., Cabell, R., Casiday, N., Cui, Z., Eicher, K., Fall, G., Feng, X., Fitzgerald, K., Frazier, N., George, C., Gibbs, R., Hernandez, L., Johnson, D., Jones, R., Karsten, L., Kefelegn, H., Kitzmiller, D., Lee, H., Liu, Y., Mashriqui, H., Mattern, D., McCluskey, A., McCreight, J. L., McDaniel, R., Midekisa, A., Newman, A., Pan, L., Pham, C., RafieeiNasab, A., Rasmussen, R., Read, L., Rezaeianzadeh, M., Salas, F., Sang, D., Sampson, K., Schneider, T., Shi, Q., Sood, G., Wood, A., Wu, W., Yates, D., Yu, W., and Zhang, Y.: NOAA's National Water Model: Advancing operational hydrology through continental-scale modeling, J American Water Resour Assoc, 1752–1688.13184, https://doi.org/10.1111/1752-1688.13184, 2024.

Do, S.K., Du, T.L.T., Lee, H. Chang, C.-H., Bui, D.D., Nguyen, N.T., Markert, K.N., Strömqvist, J., Towashiraporn, P., Darby, S.E., Bu, L.K.: Assessing impacts of Hydropower Development on Downstream Inundation Using a Hybrid Modeling Framework Integrating Satellite Data-Driven and Process-based Models, Water Resources Research, in review

Dommenget, D. and Latif, M.: A Cautionary Note on the Interpretation of EOFs, 2002.

Du, J., Kimball, J. S., Sheffield, J., Pan, M., Fisher, C. K., Beck, H. E., and Wood, E. F.: Satellite Flood Inundation Assessment and Forecast Using SMAP and Landsat, IEEE Journal of Selected Topics in Applied Earth Observations and Remote Sensing, 14, 6707–6715, https://doi.org/10.1109/JSTARS.2021.3092340, 2021.

Enayati, M., Bozorg-Haddad, O., Bazrafshan, J., Hejabi, S., and Chu, X.: Bias correction capabilities of quantile mapping methods for rainfall and temperature variables, Journal of Water and Climate Change, 12, 401–419, https://doi.org/10.2166/wcc.2020.261, 2020.

https://doi.org/10.5194/egusphere-2024-3491
Preprint. Discussion started: 15 November 2024

Farmer, W. H., Over, T. M., and Kiang, J. E.: Bias correction of simulated historical daily streamflow at ungauged locations by using independently estimated flow duration curves, Hydrology and Earth System Sciences, 22, 5741–5758, https://doi.org/10.5194/hess-22-5741-2018, 2018.

Getirana, A. C. V., Boone, A., Yamazaki, D., Decharme, B., Papa, F., and Mognard, N.: The Hydrological Modeling and Analysis Platform (HyMAP): Evaluation in the Amazon Basin, Journal of Hydrometeorology, 13, 1641–1665, https://doi.org/10.1175/JHM-D-12-021.1, 2012.

Gledhill, J. H., Barnett, A. F., Slattery, M., Willett, K. L., Easson, G. L., Otts, S. S., and Gochfeld, D. J.: Mass Mortality of the Eastern Oyster Crassostrea virginica in the Western Mississippi Sound Following Unprecedented Mississippi River Flooding in 2019, shre, 39, 235–244, https://doi.org/10.2983/035.039.0205, 2020.

Gorelick, N., Hancher, M., Dixon, M., Ilyushchenko, S., Thau, D., and Moore, R.: Google Earth Engine: Planetary-scale geospatial analysis for everyone, Remote Sensing of Environment, 202, 18–27, https://doi.org/10.1016/j.rse.2017.06.031, 2017.

Hales, R. C., Nelson, E. J., Souffront, M., Gutierrez, A. L., Prudhomme, C., Kopp, S., Ames, D. P., Williams, G. P., and Jones, N. L.: Advancing global hydrologic modeling with the GEOGloWS ECMWF streamflow service, Journal of Flood Risk Management, e12859, e12859, https://doi.org/10.1111/jfr3.12859, 2022.

Hannachi, A.: A Primer for EOF Analysis of Climate Data, 2004.

Jackson, E. K., Roberts, W., Nelsen, B., Williams, G. P., Nelson, E. J., and Ames, D. P.: Introductory overview: Error metrics for hydrologic modelling – A review of common practices and an open source library to facilitate use and adoption, Environmental Modelling & Software, 119, 32–48, https://doi.org/10.1016/j.envsoft.2019.05.001, 2019.

Kaiser, H. F.: The varimax criterion for analytic rotation in factor analysis, Psychometrika, 23, 187–200, https://doi.org/10.1007/BF02289233, 1958.

Li, S., Sun, D., Goldberg, M. D., Sjoberg, B., Santek, D., Hoffman, J. P., DeWeese, M., Restrepo, P., Lindsey, S., and Holloway, E.: Automatic near real-time flood detection using Suomi-NPP/VIIRS data, Remote Sensing of Environment, 204, 672–689, https://doi.org/10.1016/J.RSE.2017.09.032, 2018.

Li, S., Goldberg, M. D., Sjoberg, W., Zhou, L., Nandi, S., Chowdhury, N., Straka, W., Yang, T., and Sun, D.: Assessment of the Catastrophic Asia Floods and Potentially Affected Population in Summer 2020 Using VIIRS Flood Products, Remote Sensing, 12, 3176, https://doi.org/10.3390/rs12193176, 2020.

Li, S., Sun, D., Goldberg, M. D., Kalluri, S., Sjoberg, B., Lindsey, D., Hoffman, J. P., DeWeese, M., Connelly, B., Mckee, P., and Lander, K.: A downscaling model for derivation of 3-D flood products from VIIRS imagery and SRTM/DEM, ISPRS Journal of Photogrammetry and Remote Sensing, 192, 279–298, https://doi.org/10.1016/j.isprsjprs.2022.08.025, 2022.

Lorenz, E. N.: Empirical Orthogonal Functions and Statistical Weather Prediction, Massachusetts Institute of Technology, Department of Meteorology, 112 pp., 1956.

https://doi.org/10.5194/egusphere-2024-3491
Preprint. Discussion started: 15 November 2024

Markert, K. N., Chishtie, F., Anderson, E. R., Saah, D., and Griffin, R. E.: On the merging of optical and SAR satellite imagery for surface water mapping applications, Results in Physics, 9, 275–277, https://doi.org/10.1016/J.RINP.2018.02.054, 2018.

Markert, K. N., Markert, A. M., Mayer, T., Nauman, C., Haag, A., Poortinga, A., Bhandari, B., Thwal, N. S., Kunlamai, T., Chishtie, F., Kwant, M., Phongsapan, K., Clinton, N., Towashiraporn, P., and Saah, D.: Comparing Sentinel-1 Surface Water Mapping Algorithms and Radiometric Terrain Correction Processing in Southeast Asia Utilizing Google Earth Engine, Remote Sensing 2020, Vol. 12, Page 2469, 12, 2469, https://doi.org/10.3390/RS12152469, 2020.

Markert, K. N., Williams, G. P., Nelson, E. J., Ames, D. P., Lee, H., and Griffin, R. E.: Dense Time Series Generation of Surface Water Extents through Optical–SAR Sensor Fusion and Gap Filling, Remote Sensing, 16, 1262, https://doi.org/10.3390/rs16071262, 2024a.

Markert, K. N., da Silva, G., Ames, D. P., Maghami, I., Williams, G. P., Nelson, E. J., Halgren, J., Patel, A., Santos, A., and Ames, M. J.: Design and implementation of a BigQuery dataset and application programmer interface (API) for the U.S. National Water Model, Environmental Modelling & Software, 179, 106123, https://doi.org/10.1016/j.envsoft.2024.106123, 2024b.

Massey, F. J.: The Kolmogorov-Smirnov Test for Goodness of Fit, Journal of the American Statistical Association, 46, 68–78, https://doi.org/10.2307/2280095, 1951.

Nevo, S., Morin, E., Gerzi Rosenthal, A., Metzger, A., Barshai, C., Weitzner, D., Voloshin, D., Kratzert, F., Elidan, G., Dror, G., Begelman, G., Nearing, G., Shalev, G., Noga, H., Shavitt, I., Yuklea, L., Royz, M., Giladi, N., Peled Levi, N., Reich, O., Gilon, O., Maor, R., Timnat, S., Shechter, T., Anisimov, V., Gigi, Y., Levin, Y., Moshe, Z., Ben-Haim, Z., Hassidim, A., and Matias, Y.: Flood forecasting with machine learning models in an operational framework, Hydrology and Earth System Sciences, 26, 4013–4032, https://doi.org/10.5194/hess-26-4013-2022, 2022.

Pal, S., Lee, T. R., and Clark, N. E.: The 2019 Mississippi and Missouri River Flooding and Its Impact on Atmospheric Boundary Layer Dynamics, Geophysical Research Letters, 47, e2019GL086933, https://doi.org/10.1029/2019GL086933, 2020.

Rostami, A., Chang, C.-H., Lee, H., Wan, H.-H, Du, T.L.T., Markert, K.N.M., Williams, G.P., Nelson, E.J., Li, S., Straka III, W., Helfrich, S., Gutierrez, A.L.: Forecasting Flood Inundation in the U.S. Flood-prone Regions through Data-Driven Approach (FIER): Using VIIRS Water Fractions and the National Water Model, Remote Sensing, in review

Sampson, C. C., Fewtrell, T. J., Duncan, A., Shaad, K., Horritt, M. S., and Bates, P. D.: Use of terrestrial laser scanning data to drive decimetric resolution urban inundation models, Advances in Water Resources, 41, 1–17, https://doi.org/10.1016/J.ADVWATRES.2012.02.010, 2012.

Smith, A. B.: U.S. Billion-dollar Weather and Climate Disasters, 1980 - present (NCEI Accession 0209268), https://doi.org/10.25921/stkw-7w73, 2020.

Tate, E., Rahman, M. A., Emrich, C. T., and Sampson, C. C.: Flood exposure and social vulnerability in the United States, Nat Hazards, 106, 435–457, https://doi.org/10.1007/s11069-020-04470-2, 2021.

https://doi.org/10.5194/egusphere-2024-3491
Preprint. Discussion started: 15 November 2024

Teng, J., Jakeman, A. J., Vaze, J., Croke, B. F. W., Dutta, D., and Kim, S.: Flood inundation modelling: A review of methods, recent advances and uncertainty analysis, Environmental Modelling & Software, 90, 201–216, https://doi.org/10.1016/j.envsoft.2017.01.006, 2017.

Wang, Z., Bovik, A. C., Sheikh, H. R., and Simoncelli, E. P.: Image quality assessment: from error visibility to structural similarity, IEEE Transactions on Image Processing, 13, 600–612, https://doi.org/10.1109/TIP.2003.819861, 2004.

Wing, O. E. J., Lehman, W., Bates, P. D., Sampson, C. C., Quinn, N., Smith, A. M., Neal, J. C., Porter, J. R., and Kousky, C.: Inequitable patterns of US flood risk in the Anthropocene, Nat. Clim. Chang., 12, 156–162, https://doi.org/10.1038/s41558-021-01265-6, 2022.

Wing, O. E. J., Bates, P. D., Quinn, N. D., Savage, J. T. S., Uhe, P. F., Cooper, A., Collings, T. P., Addor, N., Lord, N. S., Hatchard, S., Hoch, J. M., Bates, J., Probyn, I., Himsworth, S., Rodríguez González, J., Brine, M. P., Wilkinson, H., Sampson, C. C., Smith, A. M., Neal, J. C., and Haigh, I. D.: A 30 m Global Flood Inundation Model for Any Climate Scenario, Water Resources Research, 60, e2023WR036460, https://doi.org/10.1029/2023WR036460, 2024.

Yalcin, E.: Assessing the impact of topography and land cover data resolutions on two-dimensional HEC-RAS hydrodynamic model simulations for urban flood hazard analysis, Nat Hazards, 101, 995–1017, https://doi.org/10.1007/s11069-020-03906-z, 2020.

Yamazaki, D., Kanae, S., Kim, H., and Oki, T.: A physically based description of floodplain inundation dynamics in a global river routing model, Water Resources Research, 47, 4501, https://doi.org/10.1029/2010WR009726, 2011.

Yin, S., Gao, G., Li, Y., Xu, Y. J., Turner, R. E., Ran, L., Wang, X., and Fu, B.: Long-term trends of streamflow, sediment load and nutrient fluxes from the Mississippi River Basin: Impacts of climate change and human activities, Journal of Hydrology, 616, 128822, https://doi.org/10.1016/j.jhydrol.2022.128822, 2023.